5-2018

Analysis of Thermal Properties of Permafrost, and Modeling

Mary Elizabeth Szatkowski
mszatkow@bates.edu

Analysis of Thermal Properties of Permafrost, and Modeling

MARY SZATKOWSKI

Presented to the Department of Physics & Astronomy,
and the Department of Geology,

Bates College

In partial fulfillment of the requirements for the

Degree of Bachelor of Science

Lewiston, Maine April, 2018

Acknowledgments

I would firstly like to thank my parents and brothers for fostering an environment throughout my life that has led to the enjoyment and completion of my Bates career.

I am thankful to both the faculty and students of the Bates Geology and Physics Departments for inspiring, encouraging, and aiding my pursuit of understanding the riddles of the natural world. Particular appreciation goes to my adviser, Raj Saha, for guiding me and collaborating with me throughout the entire thesis process.

My thanks goes to my closest friends, and specifically to Emily Bacon and Steven Rowe, for the network of support and fun they have provided.

Lastly, I am thankful to Gene Clough. Gene's infectious passion for constantly observing learning, and thinking is the essence that I hope to carry through my life.

> *"The power and capacity of learning exists in the soul already; and that just as the eye was unable to turn from darkness to light without the whole body, so too the instrument of knowledge can only by the movement of the whole soul be turned from the world of becoming into that of being, or in other words, of the good".*

- Platos Allegory of the Cave

Abstract

Permafrost thaw has a potentially large impact on the global climate system through release of carbon gas that has been stored as organic carbon for up to 400,000 years. System feedbacks between permafrost carbon content, microbial decomposition rates, ground temperature, and greenhouse gas radiative forcing make the permfrost system susceptible to rate induced tipping. Individual components of the permafrost system are examined to contribute to understanding of the timing and behavior of system tipping.

A Permafrost Bomb model is created to evaluate the long term decomposition ground temperature feedback behavior. Results showed several system tippings with decreasing successive amplitude under a constant atmospheric temperature forcing. This resembles the global temperature behavior of the PETM hyperthermals, supporting evidence of permafrost thaw influence on paleoclimate events. Six years of ground temperature data from a Kapp Linné borehole was analyzed for the thermal diffusivity through time and depth. Increasing atmospheric temperature is associated with greater thermal diffusivity and more effects from latent heat transfer, which were observed far below the active layer. Considering the results directly from this study and previously published research, a more complete model for permafrost is proposed. This model considers ground and

atmospheric conditions for temperature and carbon content.

Overall, these findings are applicable in permafrost and climate modeling for the purpose of understanding how the permafrost system may change and impact the global climate on both the geologic time scale and human lifespan.

Contents

Chapter 1

Introduction

1.1 Background of Permafrost

1.1.1 Permafrost Location and Extent

Permafrost is a region land, in which a portion of the subsurface remains frozen for two consecutive years (Schuur et al., 2008). It is composed of mineral soil, organic soil, rock, or ice (Schuur et al., 2008). Permafrost exists at high latitudes and elevations (Schaefer et al., 2014). In the Southern Hemisphere, it is limited to sub-antarctic islands, small regions of Antarctica, and few mountainous areas (Schaefer et al., 2014). In the Northern Hemisphere, 24 % of exposed land is characterized as permafrost (Schaefer et al., 2014). In addition to Arctic and boreal land regions, this includes areas of the continental shelf in the Arctic Ocean and high elevation subtropical regions (Schuur et al., 2008). Fig. 1.1 presents the spatial distribution of permafrost in the Northern Hemisphere. Based on the percentage of permafrost in the landscape, zones of permafrost are described as contin-

uous (90% - 100%), discontinuous (50% - 90%), sporadic (10%-50%), or isolated patches (0%-10%) (Vaks et al., 2013).

Figure 1.1: Northern Hemisphere spatial distribution of permafrost where, tan represents permafrost free areas and shades of purple represent regions of isolated, sporadic, discontinuous, or continuous permafrost cover. Figure from Schuur et al. 2008.

1.1.2 Formation

Permafrost forms when there is new soil material exposed in regions where the climate is cold enough to allow for perennially frozen subsurface material (Shur and Jorgenson, 2007). In continuous regions, formation is climate driven while, in discontinuous regions, it is dependent on climate as well as the local landscape and ecosystems (Shur and Jorgenson, 2007). Landscape processes that may result in new regions of permafrost are floodplain and drained-lake basin development (Shur and Jorgenson, 2007). In already

existing permafrost regions, syngenetic permafrost growth occurs when the local climate and landscape is unchanging due to regular sedimentation and peat formation (Schuur et al., 2008). Poor soil water drainage results in peat formation while, aeolian and alluvial processes result in sedimentation (Schuur et al., 2008). Both processes increase the elevation of the upper permafrost boundary and, therefore, permafrost depth (Schuur et al., 2008).

The high majority of permafrost present today formed during the glacial periods of the Pleistocene (Schuur et al., 2008). Higher latitude permafrost, in continuous regions, has been frozen for 400,000 years or longer (Vaks et al., 2013). Mid-latitude discontinuous permafrost regions formed during the last glacial/interglacial cycle of the Pleistocene (Schuur et al., 2008). At the last glacial maximum (LGM), approximately 20,000 years ago, permafrost coverage peaked, existing in regions of the continental United States, northern Kazakhstan, and Europe (Schuur et al., 2008). Rapid thaw, starting at the southernmost regions, occurred following the LGM such that, by the Holocene Climate Optimum, 5000 to 9000 year ago, the continental United States, western Siberia, northern Kazakhstan, and Europe, were permafrost free (Schuur et al., 2008). Permafrost thaw has continued as average global temperature has increased since the LGM (Schuur et al., 2008). New permafrost has formed n regions that are now sporadic or discontinuous permafrost during relatively cold periods of the Mid to Late Holocene (Schuur et al., 2008).

1.1.3 Temperature Profile

The temperature profile of permafrost with depth is dictated by geothermal heat and surface temperature (Osterkamp and Burn, 2003). Geothermal heat originates at Earth's core and results in an increase in temperature with ground depth (Osterkamp and Burn, 2003). The rate at which the temperature increases, the geothermal gradient, is dependent on local bedrock thermal conductivity (Osterkamp and Burn, 2003). Geothermal heat and local rock type therefore determine the depth extent of permafrost, the lower boundary being defined as the depth at which the temperature is above $0^{o}\mathrm{C}$ (Osterkamp and Burn, 2003).

The upper ground temperature is influenced from by seasonal surface temperatures (Osterkamp and Burn, 2003). Seasonal variation causes large annual temperature fluctuation in the upper region of permafrost, resulting in a distinct winter and summer permafrost profile (Osterkamp and Burn, 2003). In the Northern Hemisphere winter, the surface temperature is less than $0^{o}\mathrm{C}$. Ground temperature increases rapidly from the surface with depth until it aligns with the expected temperature based on the geothermal gradient. It then continues to increase with depth by the geothermal gradient. In the summer, the surface temperature is above $0^{o}\mathrm{C}$. Ground temperature decreases rapidly with depth until it aligns with the geothermal gradient, at which point it will increase with depth by the geothermal gradient.

The topmost portion of the ground, due to surface temperature, thaws in the summer and freezes in the winter (Osterkamp and Burn, 2003). This region is the active layer, defined as the greatest depth that is above $0^{o}\mathrm{C}$ at any point in the year (Osterkamp and

Burn, 2003). The upper boundary of the permafrost is at the base of the active layer (Osterkamp and Burn, 2003). The region between the active layer and stable permafrost is particularly ice-rich and is defined as the transition zone (Osterkamp and Burn, 2003). Fig. 1.2 graphically represents the general permafrost temperature profile with depth.

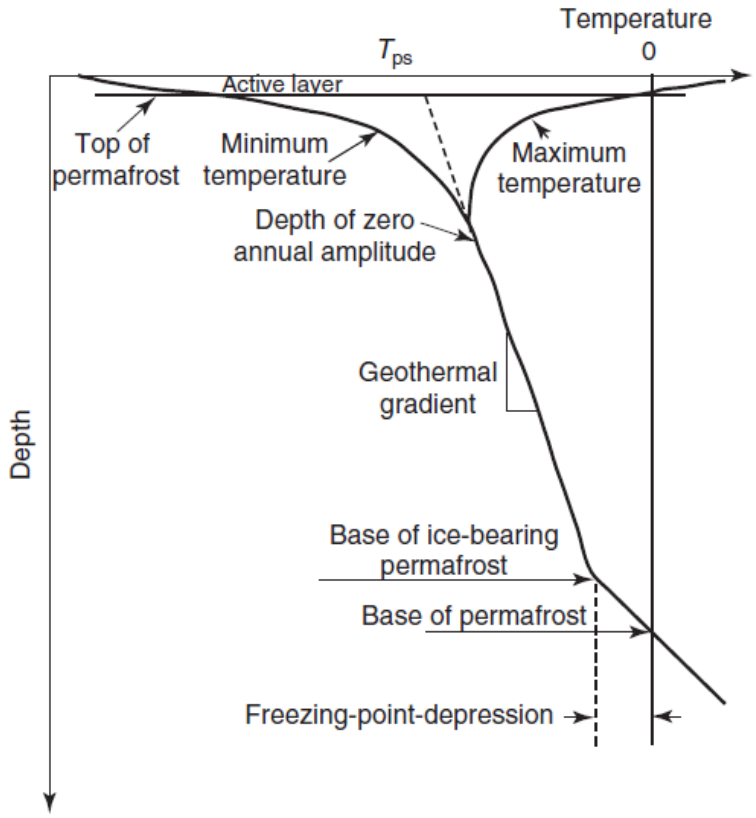

Figure 1.2: Permafrost depth temperature profile annotated with the summer profile (maximum temperature), winter profile (minimum temperature), active layer, permafrost bounds, and geothermal gradient. Figure from Osterkamp and Burn, 2003.

While seasonal atmospheric temperature changes hardly influence permafrost temperature at great depth, long term atmospheric trends do impact permafrost temperature at depth. Fig. 1.3 presents the annual average temperature at a borehole on Ellesmere Island from 1978 to 2014 at 24.4m deep. The temperature has increased from about -15.5°C to -13°C since 1978, with a greater rate of increase after 2000. Fig. 1.4 shows the

monthly average temperature from a borehole in Igloolik, Nunavut from 2008 to 2011 at 15m depth. Even in these three years, an increase in temperature is observed. The fact that these great depths are reflecting the atmospheric temperature change over a relatively short time period shows one example of how the permafrost temperature profile will be affected by warming of the global climate.

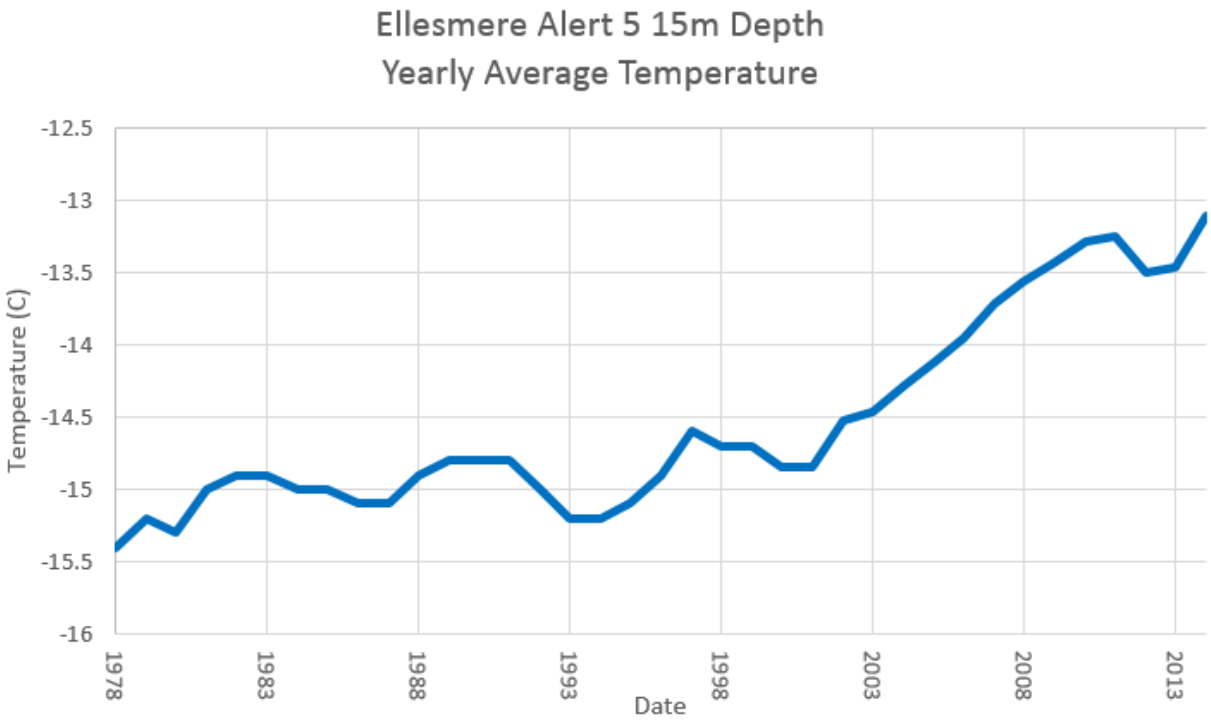

Figure 1.3: Permafrost annual ground temperature data from the Ellesmere Alert 5 borehole at 24.4m depth from 1978 to 2014. Data is from the GTNP.

The temperature at any specific depth in the permafrost is impacted by the temperatures at higher and lower depths via heat conductivity (Frob, 2011). Heat conductivity is dependent on material characteristics, thermal conductivity and specific heat capacity (Frob, 2011). Both of these properties vary based on the ground lithologic composition, water content, ice content, and air content (Woo, 2012). As temperature is a controlling factor of water and ice content, it ultimately influences the thermal conductivity and heat

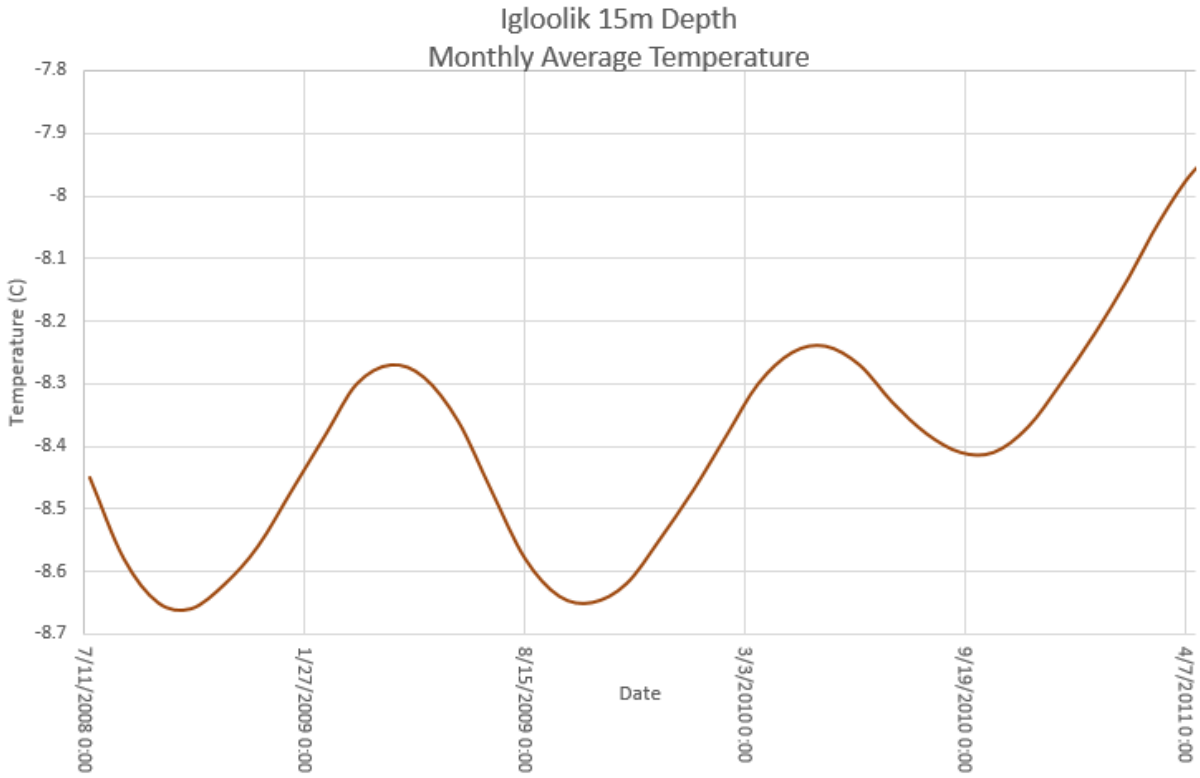

Figure 1.4: Permafrost monthly ground temperature data from the Igloolik borehole at 15m depth from 2008 to 2011. Data is from the GTNP.

capacity of permafrost (Woo, 2012). This means that these thermal properties vary with location and time.

1.1.4 Carbon Storage

The organic and mineral soil in permafrost acts as a carbon reservoir in the global carbon cycle (Schuur et al., 2008). Peat, organic rich soil is 20% to 60% carbon and mineral soil is 0% to 20% carbon (Schuur et al., 2008). The carbon originates from plant photosynthesis and growth, resulting in highest carbon density in permafrost in the shallow most depths (Schuur et al., 2008). Methods of syngenetic permafrost growth and cryoturbation encourage movement of the organic carbon from the uppermost permafrost to

lower depths, where it is more likely to remain frozen and undecomposed (Schuur et al., 2008). Syngenetic permafrost growth increases the amount of material above the previously deposited organics, burying the organics into the permafrost (Schuur et al., 2008). Cryoturbation is the mixing of deposited soils due to repeated freezing and thawing of the ground (Schuur et al., 2008). This mixing moves organics from the uppermost ground layer to permafrost depths (Schuur et al., 2008).

Decompositional processes in soil release the organic carbon stored as carbon dioxide and methane (Walz et al., 2017). Microbial decomposition is dependent, namely, on carbon availability, temperature, and oxygen availability (Hollesen et al., 2015). In permafrost regions, the temperature is often too low for significant decomposition of the stored organic carbon to take place (Walz et al., 2017). Under somewhat warmer temperatures, permafrost is often saturated with water due to ice melt or precipitation, limiting oxygen availability for decomposition (Schuur et al., 2008). Due to the lack of organic decomposition as peat formation and sedimentation continue over time, the organic carbon stored in permafrost accumulates (Schuur et al., 2008). It is estimated that 1700Gt of organic carbon is stored in Northern Hemisphere permafrost (Vaks et al., 2013). Over 60% of this organic carbon is within the upper 3m of global permafrost (Koven et al., 2009). Increase in permafrost temperature generally encourages microbial decomposition and therefore leads to the release of organic carbon in permafrost, as carbon dioxide and methane gas, into the atmosphere (Christensen et al., 2004).

1.2 Role of Permafrost in the Global Climate

1.2.1 Carbon Cycle and Global Climate

There is a positive feedback between atmospheric temperature and greenhouse gas concentration. Greenhouse gases in the Earths atmosphere absorb radiation emitted from the Earth, trapping heat within the atmosphere and increasing the temperature (Hansen et al., 1981). Greater temperatures encourage greenhouse gas concentrations through increased evaporation rates and variety of processes specific to individual greenhouse gasses. Carbon dioxide, a prevalent greenhouse gas, has several feedback with atmospheric temperature through the carbon cycle (Hogg, 2008). This relationship is reflected in records of atmospheric temperature and carbon dioxide concentration, as the two variables covary through Earths major climate cycle (Hogg, 2008). Fig. 1.5 graphically shows the global temperature and carbon dioxide values interpreted from Antarctic ice cores for the last 400,000 years. The major components on the geologic time scale of the global temperature and carbon dioxide feedback are silicate weathering, ocean out-gassing, vegetation, and the greenhouse gas radiative effect (Hogg, 2008).

In the past 140 years, there has been significant anthropogenic influence on atmospheric greenhouse gas concentrations due to the burning of fossil fuels (Schaefer et al., 2014). Fig. 1.6 graphically shows the measured values of atmospheric carbon dioxide and global temperature since 1958. The increasing trend of atmospheric carbon dioxide concentration and temperature on this time scale is reflective of the anthropogenic input of carbon into the atmosphere from the pre-industrial average of 280ppm to the current value of 400ppm and its effect on the global temperature (NOAA, 2018). The

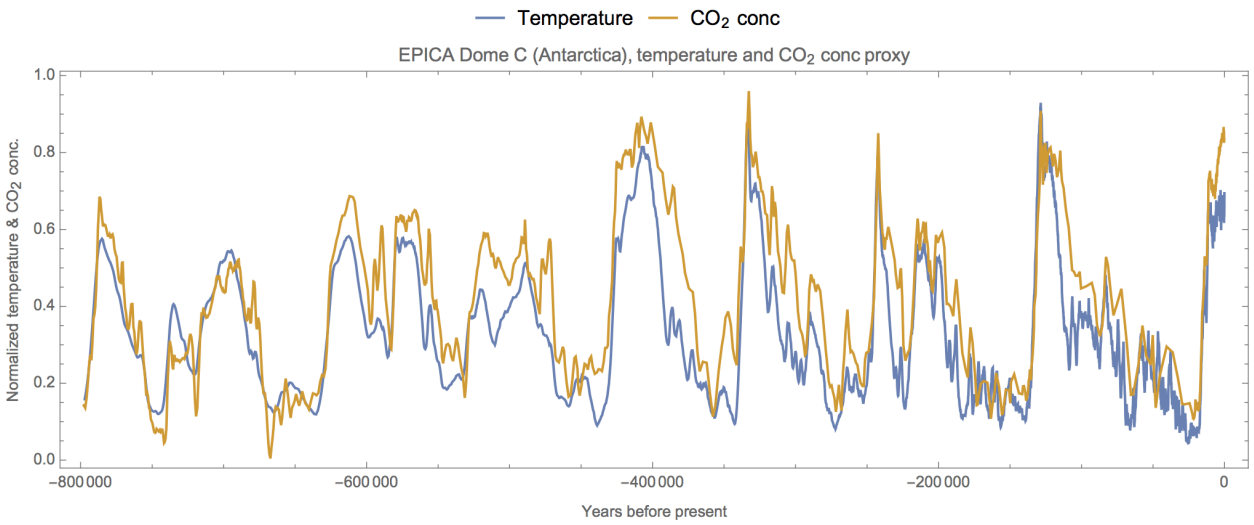

Figure 1.5: Graph of global atmospheric temperature anomaly (°C), blue, and carbon dioxide concentration (ppm), orange, from about 800,000 years ago to present. Data constructed from EPICA Dome, Antarctica.

estimated permafrost reservoir organic carbon storage, 1700Gt, is almost twice as much as that currently in the atmosphere (Schaefer et al., 2014). Therefore, input to the atmosphere from the permafrost system, which is temperature sensitive, could significantly impact the Earth's immediate climate (Schaefer et al., 2014).

1.2.2 Permafrost Thaw and Paleoclimate

There is evidence that permafrost thaw has occurred at various points throughout Earth's history in coincidence with global climate warming anomalies. Speleothem growth history in Siberian caves reflect permafrost thaw extent over the past 500,000 years (Vaks et al., 2013). Regions of permafrost currently characterized as discontinuous and sporadic experienced thaw during each of six interglacial periods in the last 500,000 years, including the present (Vaks et al., 2013). Regions currently continuous permafrost, at 60°N, only have recorded thaw during MIS 11, about 400,000 years ago (Vaks et al., 2013). MIS 11,

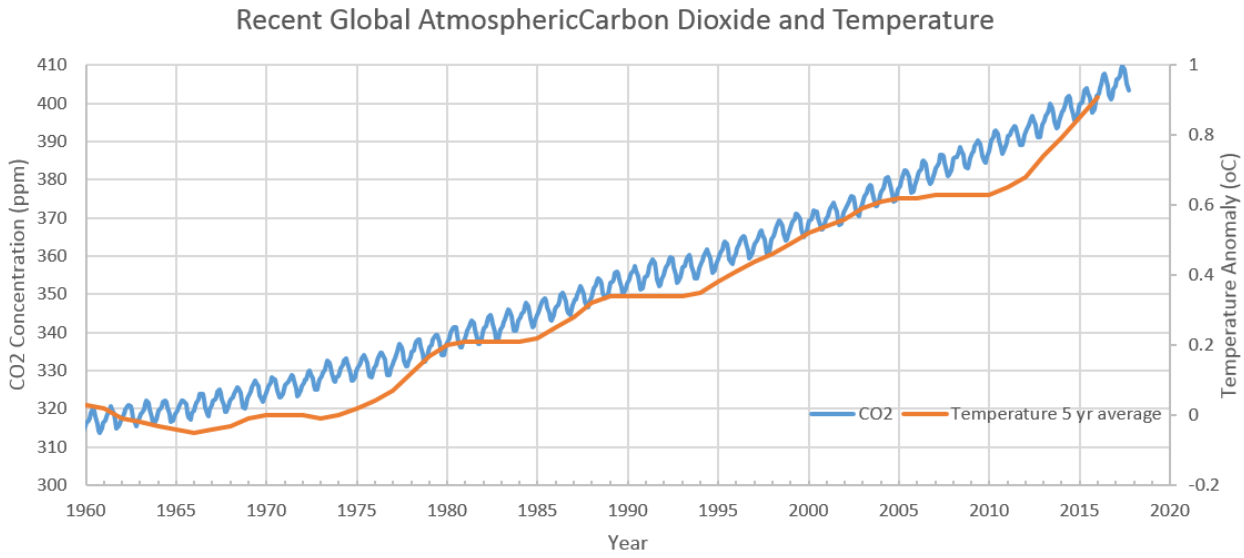

Figure 1.6: Measured atmospheric carbon dioxide and global temperature from 1958 to present. Temperature is presented yearly as a 5 yr average and carbon dioxide is given monthly. Data from NOAA, 2017.

therefore, represents the most significant permafrost thaw event in the past 500,000 years, which aligns with other Quaternary climate proxies (Vaks et al., 2013). The MIS 11 interglacial corresponds with a local temperature 4°C to 5°C warming than today, and a global average 1.5°C higher than present (Vaks et al., 2013).

It is hypothesized that, not only did permafrost thaw in the Quaternary interglacials, but also that the resulting carbon gas release from organic carbon decomposition may have contributed to both the timing and extent of the interglacials (Zech, 2012). Previously, it has been determined that the difference between atmospheric carbon dioxide concentration during glacials, 180-200 ppm, and interglacials, 250-300 ppm, was due to ocean carbon storage and outgassing (Zech, 2012). However, considering all possible ocean carbon storage changes, ocean processes alone do not account for the range of carbon dioxide in the atmosphere from glacials to interglacials (Zech, 2012). Additionally, this determination assumed that no terrestrial carbon storage would increase during

glacials (Zech, 2012).

The Tumara permafrost profile sequence has organic rich layers attributed to glacial periods and organic poor layers attributed to interglacial periods (Zech, 2012). This shows that permafrost acts as a greater net carbon storage during glacials, when slow carbon sequestration is possible, than interglacials, when carbon is released through decomposition processes (Zech, 2012). The carbon storage and release from permafrost likely accounts for a portion of the glacial to interglacial atmospheric carbon dioxide difference, impacting the global climate extent Quaternary glacial cycles (Zech, 2012).

On a larger timescale, permafrost thaw has been proposed as the cause of the series of extreme warming events, hyperthermals, between 55 and 52.5 million years ago (DeConto et al., 2012). These events followed the Palaeocene-Eocene Thermal Maximum (PETM), in which global mean temperature increased by about $5^{o}\mathrm{C}$ over only a few thousand years (DeConto et al., 2012). At that time, orbital forcings of high eccentricity and obliquity were driving long-term global warming, with intensified effects on high latitudes (DeConto et al., 2012). It is therefore likely that the cause of the hyperthermals was related to global temperature and sensitive to polar climates, such as permafrost (DeConto et al., 2012). Permafrost regions may have reached a climatic threshold at the PETM which induced rapid thaw and out-gassing of carbon (DeConto et al., 2012). Increase in silicate weathering rates and gradual restock of the permafrost carbon allowed for climate recovery after the PETM and hyperthermals until orbital forcings, again, triggered permafrost system tipping and climate hyperthermal (DeConto et al., 2012). Permafrost systematic thaw and re-establishment align with the observed decrease in intensity of successive hyperthermals, as the permafrost would not recover all of the original carbon stored be-

tween hyperthermals (DeConto et al., 2012). This scenario represents the potentially large impact that the permafrost system can have on the global climate.

1.2.3 System Feedbacks

The permafrost system is composed of multiple feedback relationships that dictate system reaction to condition changes (Hollesen et al., 2015). The major feedback processes are microbial decomposition rates, greenhouse gas radiative forcing, and internal heat production (Hollesen et al., 2015). Microbial decomposition converts organic carbon to carbon gas, namely carbon dioxide or methane, which is released into the atmosphere (Treat et al., 2014). Decomposition rate within permafrost is dependent on the ground temperature and organic carbon content (Schuur et al., 2008). This process has a negative feedback between decomposition rates and carbon content, as the continuation of decomposition will deplete the permafrost carbon storage and therefore decrease decomposition rate (Hollesen et al., 2015). Internal heat production refers to microbial decomposition processes which release heat and increase the surrounding ground temperature (Hollesen et al., 2015). Decomposition rate increases with temperature, until some maximum productivity level, and then decreases with temperature (Pietikainen et al., 2004). The internal heat production decomposition rate relationship most readily acts as a positive feedback due to the currently low permafrost temperatures but, could act as a negative feedback after some maximum productivity temperature.

Carbon gas released to the atmosphere through microbial decomposition acts as a greenhouse gas, increasing the atmospheric temperature through greenhouse gas radia-

tive forcing (Crichton et al., 2014). Increase in atmospheric temperature corresponds to an increase in permafrost ground temperature, which impacts the decomposition rates (Hollesen et al., 2015). Again, this feedback could either be positive or negative, depending on the initial temperature of the system. Fig. 1.7 is a schematic diagram of the feedback relationships within the permafrost system. Fig. 1.7 notes both internal heat production and greenhouse gas radiative forcing as positive feedbacks with decomposition rates because, current permafrost temperatures are lower than the bacterial maximum decomposition rate (Treat et al., 2014).

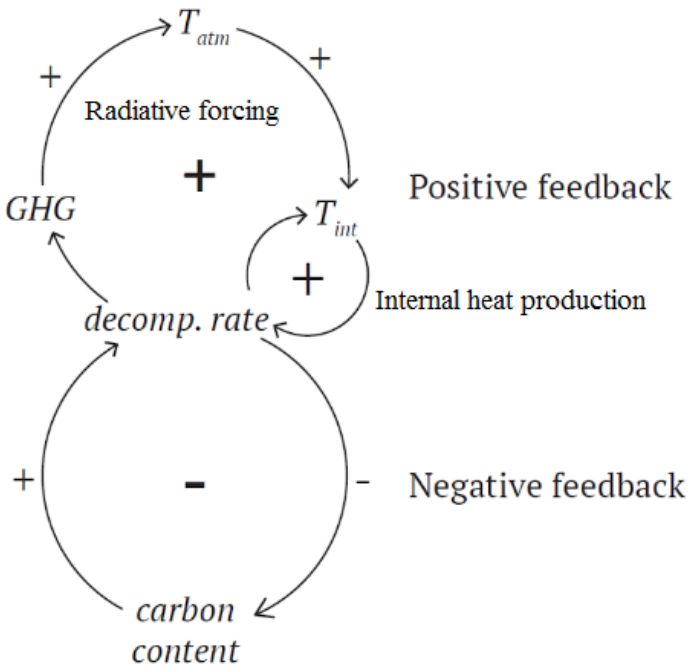

Figure 1.7: Simplified diagram depicting the feedbacks in the permafrost system. Arrows accompanied with positive or negative signs represent the effect of one variable on another. Positive or negative symbols inside of a feedback loop represent the system feedback effect as a whole.

1.2.4 System Tipping

The presence of positive feedback cycles within the permafrost system causes there to be great sensitivity to condition changes (Hoyer-Leitzel et al., 2017). Such sensitivity results in the possibility of system tipping, when small changes in external conditions result in large change in system conditions or behavior (Hoyer-Leitzel et al., 2017). Typically, tipping is considered to be threshold induced, in which the system will tip when a system variable is above a specific value (Wieczorek et al., 2010). Systems with internal positive feedbacks, however, may be better represented with a rate-induced tipping mechanism, in which the rate of which conditions change, rather than their instantaneous value, dictates system tipping (Hoyer-Leitzel et al., 2017). As positive and negative feedbacks are the basis of many systems in the global climate, rate-induced tipping approach of representation and understanding is applicable within many aspects of the Earth's climate system (Hoyer-Leitzel et al., 2017). This concept is additionally reflective of ecosystem adaptability to small condition changes through time (Shur and Jorgenson, 2007).

Wieczorek et al., 2010 applied the concept of rate-induced tipping to a peatland fire scenario in the Compost Bomb Instability model, which considered the positive feedback between peatland decomposition and ground temperature (Wieczorek et al., 2010). The model evaluates the effect of a constant rate of atmospheric temperature change, independent of the other variables, on the peatland ground temperature and carbon content, which are coupled (Wieczorek et al., 2010). The Compost Bomb Instability model predicts a threshold rate of atmospheric temperature increase (Wieczorek et al., 2010). Below this rate, the peatland ground temperature remains relatively stable but, above, the ground

temperature rapidly increases, signifying system tipping (Wieczorek et al., 2010).

The permafrost system is directly analogous to the Compost Bomb Instability model through the decomposition rate ground temperature feedback and atmospheric temperature dependence of ground temperature. The permafrost system has the additional feedback between the ground and atmospheric conditions through the greenhouse gas radiative forcing. Therefore, the permafrost system may be best represented by a rate-induced tipping mechanism. Rate-induced tipping of the permafrost system would be rapid permafrost thaw in response to a small increase of atmospheric temperature or carbon content change rate.

1.3 Purpose of Study

1.3.1 Adapting "Compost Bomb" Model for Permafrost

The purpose of this study is to explore critical transitions within the permafrost system, product of the system feedbacks, through numerical models. Firstly, the Compost Bomb Instability model from Wieczorek et al. 2010 will be directly modified and refined to better represent the permafrost system. The model is composed of differential equations for atmospheric temperature, ground carbon content, and ground temperature, where ground conditions are considered for a single permafrost layer. This model focuses on the ground temperature decomposition rate feedback with a year time step, which allows for evaluation of the long term trends and responses of this feedback alone. Model specifications that differ for the permafrost system from the peatland representation in

the the Compost Bomb Instability model are ground thermal properties, decomposition rate, litter deposition rate, and the initial conditions of ground temperature and carbon content.

1.3.2 Thermal Properties

The temperature profile of permafrost throughout time is largely defined by the thermal conductivity and specific heat capacity of the permafrost (Osterkamp and Burn, 2003). It has been previously recognized that these values depend on the permafrost lithology, water content, and ice content (Woo, 2012). How the thermal conductivity to heat capacity ratio, $\mathrm{d_h}$, varies in a single permafrost location through time, however, has not been explicitly described. This study analyzes permafrost ground temperature data from two boreholes to develop a numerical function to describe $\mathrm{d_h}$ in terms of time, temperature, and depth. The purpose of a well defined $\mathrm{d_h}$ function is to increase understanding of the general permafrost system and, can be applied within permafrost system models to produce more accurate model representations.

1.3.3 A More Complete Model

Secondly, a numerical model that considers the feedback between the ground and atmospheric conditions in addition to internal heat production will be proposed. This model will more accurately represent the permafrost system and offer greater information to the effect of permafrost thaw on the global climate. The use of small time steps allows for evaluation of permafrost behavior throughout a year and also puts this model in refer-

ence to the human lifespan. Both the internal heat production and greenhouse gas radiative forcing feedback mechanisms have been considered separately in previous models but, the coupling of the two systems for a complete view of the system has not been done. This will require equations of state for atmospheric temperature, atmospheric carbon concentration, ground temperature, and ground carbon content. Ground conditions are considered for multiple finite permafrost layers.

1.3.4 Relevance

Anthropogenic greenhouse gas input has contributed to to rise of atmospheric carbon dioxide from preindustrial 280 ppm to the current 400 ppm and has led to global temperature rise (IPPC, 2014). Understanding climate systems and their tipping points is vital to recognizing how local and global environments may change in response. This information is essential when creating and implementing climate mitigation policies in response to the anthropogenic influence of the rapidly changing climate (Schaefer et al., 2014). Current global climate policies do not consider the influence of permafrost thaw on the climate system (Schaefer et al., 2014). Permafrost, however, could play a major role in the global climate due to its large carbon storage and potential for rate-induced tipping. The three focuses of this study will offer greater understanding of the permafrost system in reference to regular heat flow, the long term ground temperature decomposition rate feedback through internal heat production, and the interaction between the permafrost and global climate systems. In combination, this will allow for more accurate permafrost model representations in the future and, ultimately, better recognition of the

effect of current climate change on near future climate conditions through the permafrost system feedbacks.

Chapter 2

"Permafrost Bomb" Model

2.1 The "Compost Bomb Instability" Model

2.1.1 Equations of State

The Compost Bomb Instability model, from Wieczorek et al., 2010, is a three dimensional system of differential equations made to represent the peatland temperature decomposition rate feedback (Wieczorek et al., 2010). Equations of state are given to represent atmospheric temperature, $\mathrm{T_a}$, ground temperature, T, and ground carbon content, C. Eq. 2.1 gives the equation for ground carbon content where, L is annual litter fall and $r(T)$ is the rate of microbial decomposition. A temperature dependent function for microbial decomposition rate is given in Eq. 2.2, where r_0 and α are constants. Note that this is an exponential function. Eq. 2.3 is the rate of ground temperature change in which, μ is the heat capacity, A is a constant of proportionality, and k is the thermal conductivity. The

rate of atmospheric temperature change, Eq. 2.4, is set to a constant positive value, v.

$$\frac{dC}{dt} = L - Cr(T) \tag{2.1}$$

$$r(T) = r_0 \exp(\alpha T) \tag{2.2}$$

$$\mu \frac{dT}{dt} = ACr(T) - k(T - T_a) \tag{2.3}$$

$$\frac{dT_a}{dt} = v \tag{2.4}$$

Hoyer-Leitzel et al., 2017 ran the Compost Bomb Instability model for varying values of v to observe the rate-induced system tipping. Table 2.1 lists all constants in the Compost Bomb Instability model used by Hoyer-Leitzel et al., 2017. The initial system conditions are (50 $\mathrm{kg\,m^{-2}}$, 8.15$^{\mathrm{o}}$C, 0$^{\mathrm{o}}$C) for (C, T, $\mathrm{T_a}$).

L	$1.055\,\mathrm{kg\,m^{-2}\,yr^{-1}}$
α	$0.1\ln(2.5)\,\mathrm{C^{-1}}$
k	$5.049 \times 10^6\,\mathrm{J\,yr^{-1}\,m^{-2}\,C^{-1}}$
r_0	$0.01\,\mathrm{yr^{-1}}$
μ	$7.8 \times 10^6\,\mathrm{J\,m^{-2}\,C^{-1}}$
A	$3.9 \times 10^7\,\mathrm{J\,kg^{-1}}$

Table 2.1: Parameters for Compost Bomb Instability Model as used in Hoyer-Leitzel et al., 2017.

2.1.2 Dynamical Behavior

Results from the Compost Bomb Instability model for v values of 0.07$^{\mathrm{o}}\mathrm{Cyr^{-1}}$, 0.1$^{\mathrm{o}}\mathrm{Cyr^{-1}}$, and 0.11$^{\mathrm{o}}\mathrm{Cyr^{-1}}$ were calculated. Fig. 2.1 and Fig. 2.2 show the results from the Compost

Bomb Instability for ground temperature and ground carbon content, respectively. An atmospheric temperature change rate of 0.1 $^{o}\mathrm{Cyr}^{-1}$ perturbs the system slightly while, an atmospheric temperature change rate of 0.11 $^{o}\mathrm{Cyr}^{-1}$ results in a rapid release of all ground carbon and increase in ground temperature. This is representative of the rate-induced tipping of the peatland system.

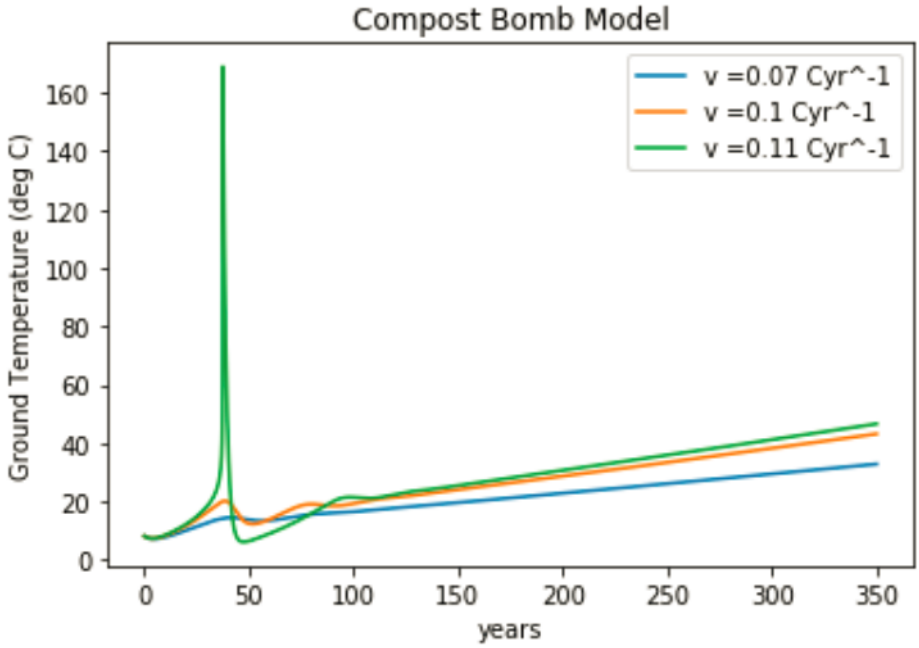

Figure 2.1: Ground temperature results from the Compost Bomb Instability model for v values of 0.07, 0.01, and 0.11 $^{o}\mathrm{Cyr}^{-1}$

2.2 Adaptation of "Compost Bomb" for Permafrost

2.2.1 Temperature Dependence of Soil Microbial Decomposition

Wieczorek et al., 2010 proposes an exponential temperature dependence of the decomposition rate function for peatlands, defining $r(T) = 0.01e^{0.091T}$ $\mathrm{kgCkgC}^{-1}\mathrm{yr}^{-1}$. Treat et al., 2014 and Mikan et al., 2002 both did lab analysis of the decomposition rates of organic

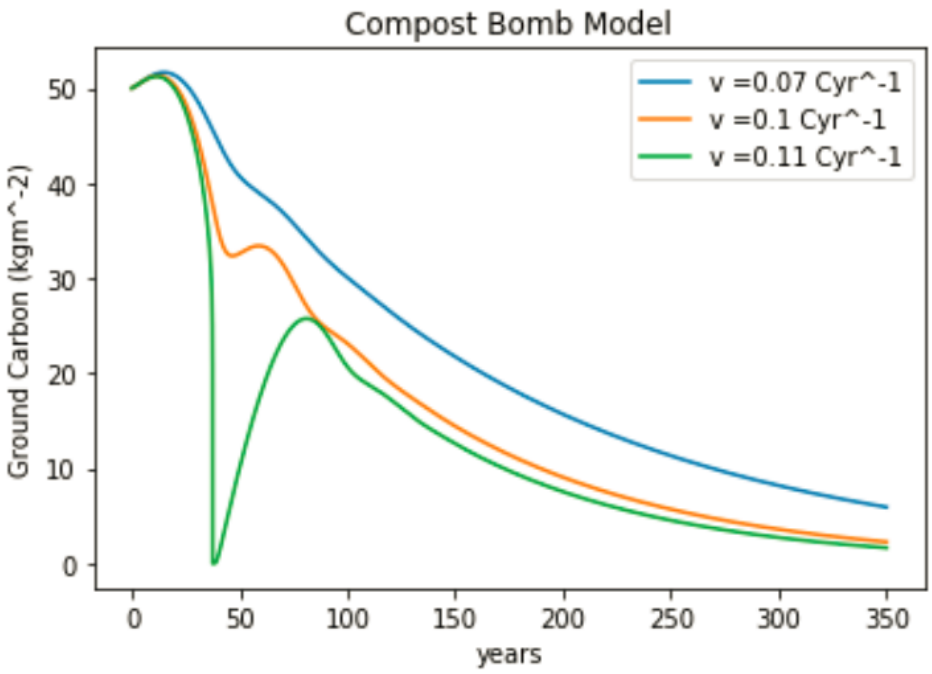

Figure 2.2: Ground carbon density results from the Compost Bomb Instability model for v values of 0.07, 0.01, and 0.11 $^{o}\mathrm{Cyr}^{-1}$

rich soil from permafrost active layers under a range of temperatures. Both determined that an exponential decomposition rate function best fit their data. However, Treat et al., 2014 analyzed sample decomposition at only four temperatures between -5^{o}C and 20^{o}C. Due to the limited number of data points and small range of tested respiration temperatures, the temperature dependence of the decomposition rate, especially at higher temperatures, is not clear. Mikan et al., 2002 recorded decomposition at fourteen different temperatures but, still only covered a range from -10^{o}C to 14^{o}C. There were enough data points to conclude a decomposition function over the tested temperature range but, still, the decomposition rate at higher temperatures is left unknown.

Pietikainen et al., 2004 performed lab respiration analysis on soils and fungus, not specific to arctic regions, for a temperature range from 0^{o}C to 40^{o}C. Fig. 2.3, the respiration results for humus soil from their study, shows that respiration rates exhibit exponential

temperature dependence at relatively low temperatures but, do not continue this trend towards higher temperatures (Pietikainen et al., 2004). Rather, there is some maximum temperature, after which the decomposition rates are impeded by greater temperatures (Pietikainen et al., 2004). A Gaussian function is representative of this mechanism. Fig. 2.4 shows the results from Pietikainen et al., 2004 of relative bacterial activity in humus soil over the same temperature range. This fully shows a Gaussian curve, as bacterial activity decreases significantly at greater temperatures (Pietikainen et al., 2004). While decomposition rates in permafrost have previously been defined as exponential functions, this representation is unrealistic based on typical bacterial activity behavior as represented in Pietikainen et al., 2004. Therefore, a Gaussian function would better represent the temperature dependence of permafrost decomposition rate.

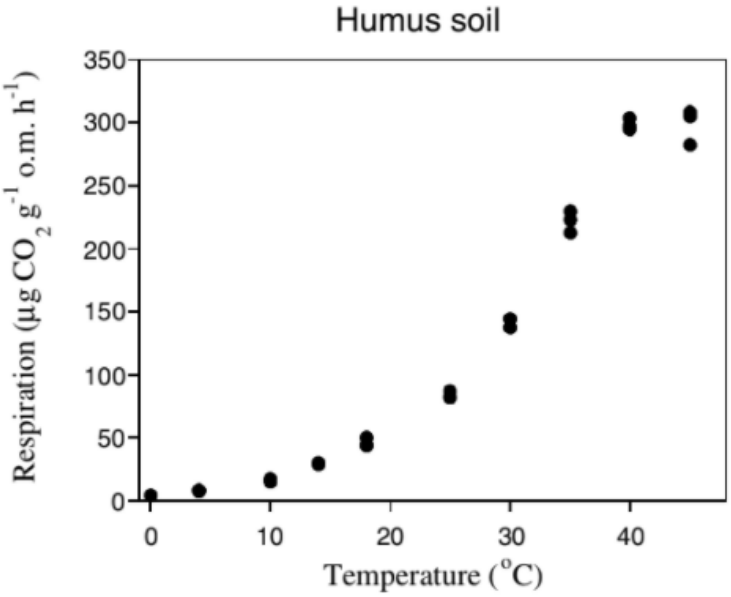

Figure 2.3: Respiration of humus soil for 0°C through 40°C. Peak respiration rate occurs at about 40°C. Figure from Pietikainen et al., 2004.

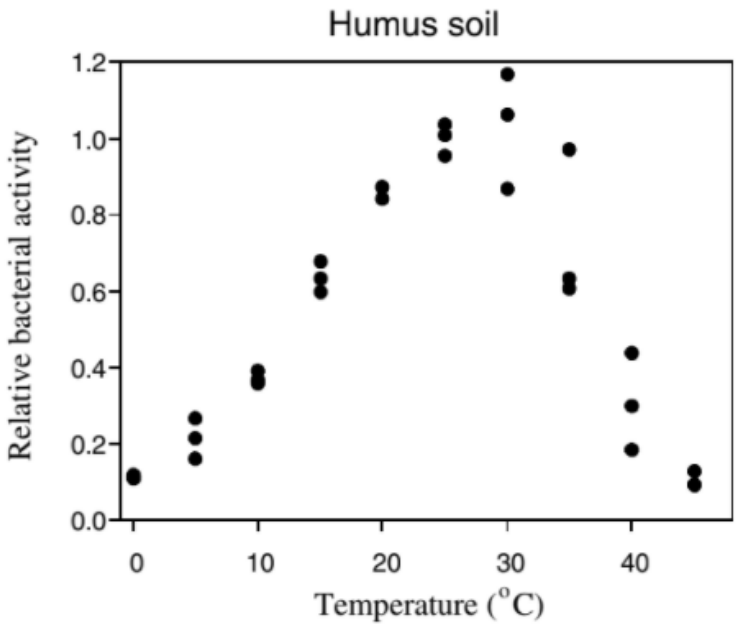

Figure 2.4: Relative bacterial activity in humus soil from 0°C through 40°C. Peak bacterial activity occurs at about 25°C. Figure from Pietikainen et al., 2004.

2.2.2 Modeling Soil Microbial Decomposition

To determine a Gaussian function representative of permafrost decomposition, an estimated Gaussian function is compared to the proposed exponential decomposition rate functions, $r(T)$, in Wieczorek et al., 2010, Treat et al., 2014, and Mikan et al., 2002. These functions take the form of Eq. 2.2, with varied values for r_0 and α. Eq. 2.5 shows a Gaussian decomposition rate function. This equation has three parameters; $\mathrm{T_c}$, a, and b. $\mathrm{T_c}$ is the maximum decomposition temperature and a and b are constants that determine the shape of the Gaussian curve. The functions are compared critically only up to 20°C, as this was the highest temperature supported by a lab measurement.

$$r(T) = \frac{a}{\sqrt{2\pi}} \exp(\frac{-b}{2}(T - T_c)^2) \tag{2.5}$$

Fig. 2.5 and Fig. 2.7 present Gaussian functions that reasonably fit the previously proposed exponential functions within the 0°C to 20°C test window. The estimated Gaussian

function presented in Fig. 2.8, with a T_c of 40°C, is similar in amplitude and central temperature to the respiration rates measured in humus soil by Pietikainen et al., 2004, shown in Fig. 2.3. The estimated Gaussian curve in Fig. 2.6, with a T_c of 70°C, does not align with any specific measurements beyond the 0°C to 20°C test window but, is informative to consider as the temperature dependence of permafrost decomposition rates is very unclear above 20°C. Fig. 2.6 and Fig. 2.8 compare the newly proposed Gaussian decomposition functions to the previously used exponential decomposition functions over a temperature range up to 100°C. In the adaptation of the Compost Bomb Instability model into a Permafrost Bomb model, the estimated Gaussian functions in both Fig. 2.6 and Fig. 2.8 will be used as $r(T)$, rather than an exponential function.

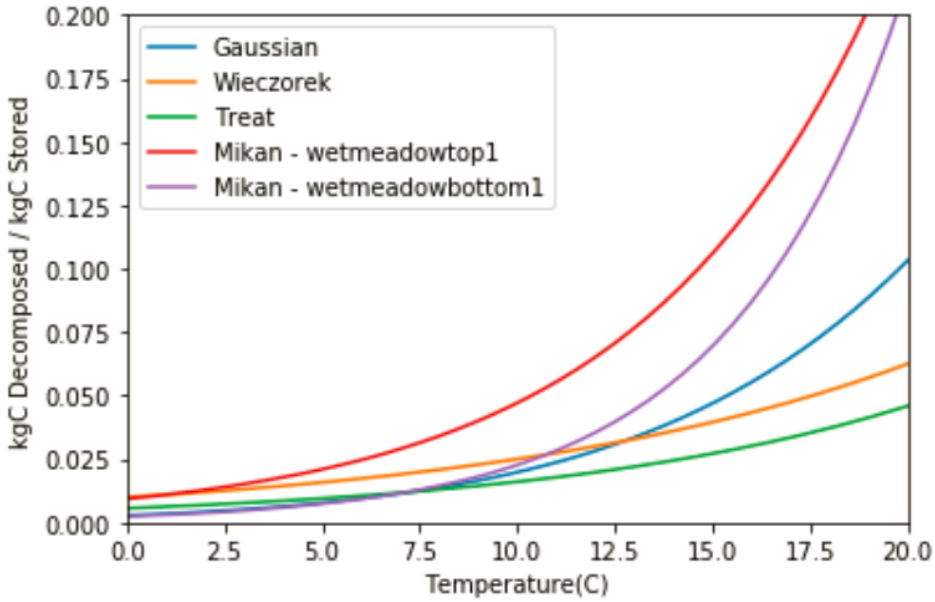

Figure 2.5: Comparison of $r(T)$ functions from 0°C to 20°C, the highest temperature with function supporting lab measurement. Gaussian parameters are T_c = 70°C, $a = 11$, and $b = 0.003$.

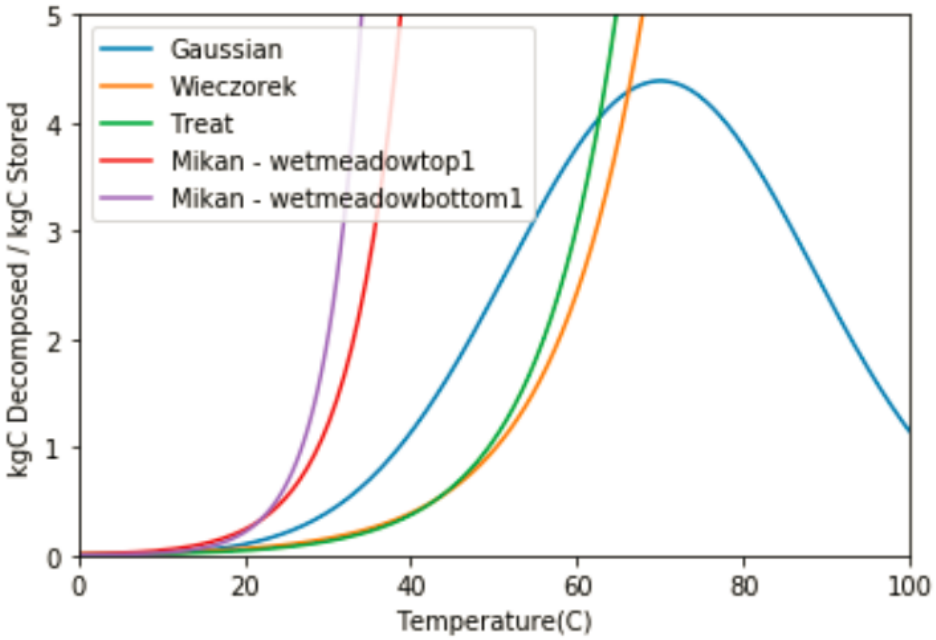

Figure 2.6: Comparison of $r(T)$ functions from 0°C to 100°C. Gaussian parameters are $\mathrm{T_c}$ = 70°C, $a = 11$, and $b = 0.003$.

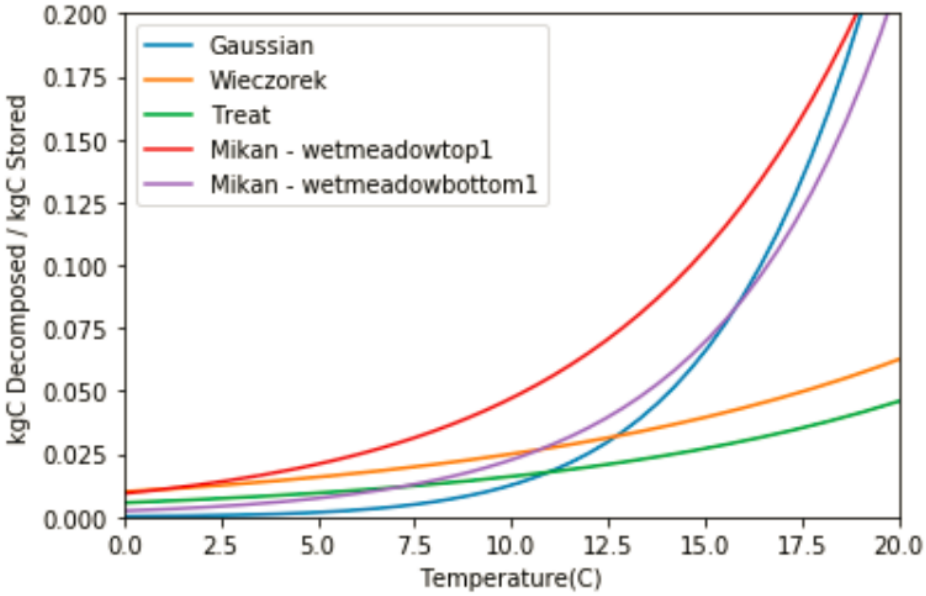

Figure 2.7: Comparison of $r(T)$ functions from 0°C to 20°C, the highest temperature with function supporting lab measurement. Gaussian parameters are $\mathrm{T_c}$ = 40°C, $a = 7$, and $b = 0.012$.

2.2.3 Initial Conditions

Initial conditions used in Wieczorek et al., 2010 Compost Bomb Stability model for peatlands are (50 $\mathrm{kgm^{-2}}$, 8.15°C, 0°C) for (C, T, Ta). These conditions are different for a per-

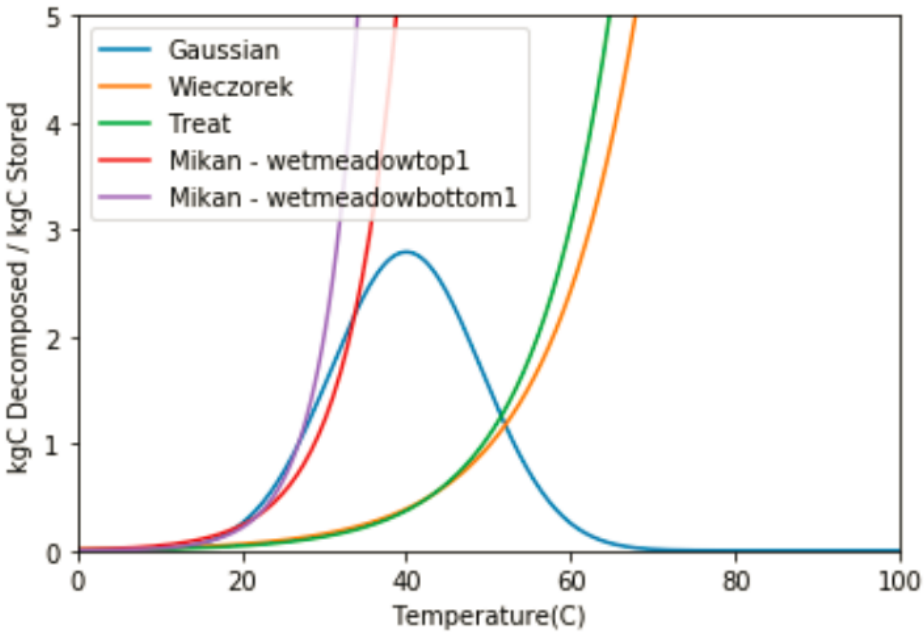

Figure 2.8: Comparison of $r(T)$ functions from 0°C to 100°C. Gaussian parameters are $\mathrm{T_c}$ = 40°C, $a = 7$, and $b = 0.012$.

mafrost specific Permafrost Bomb model. Ground temperature data for a borehole in Kapp Linné, Svalbard, Norway shows that the annual average atmospheric temperature and ground temperature at that location has been -3°C for six years (Christiansen, 2016). As many other permafrost regions exist in a similar climate, this will be used as the initial condition for both atmospheric and ground temperature in the Permafrost Bomb model. Ground carbon content will be considered for organic rich permafrost, such as those sampled in Treat et al., 2014. The average soil carbon content sampled from both the active layer and upper permafrost from locations spread across Alaska in Treat et al., 2014 was $58\mathrm{kgm}^{-2}$, and will therefore be used as the initial condition for ground carbon in the Permafrost Bomb model.

2.2.4 Dynamical Behavior

The Permafrost Bomb model was run with the same specifications as the Compost Bomb Instability model in Hoyer-Leitzel et al., 2017 except, with the decomposition function given in Eq. 2.5 with Gaussian parameters described in Fig. 2.6 and Fig. 2.8 and updated initial conditions. Figures 2.9, 2.10, and 2.11 show the results from a Gaussian decomposition function with a $\mathrm{T_c}$ of 70$^{\mathrm{o}}\mathrm{C}$ for a v of 0.0 $^{\mathrm{o}}\mathrm{Cyr}^{-1}$, 0.02 $^{\mathrm{o}}\mathrm{Cyr}^{-1}$, and 0.06 $^{\mathrm{o}}\mathrm{Cyr}^{-1}$, respectively. Figures 2.12, 2.13, and 2.14 show the results from a Gaussian decomposition function with a $\mathrm{T_c}$ of 40$^{\mathrm{o}}\mathrm{C}$ for a v of 0.01 $^{\mathrm{o}}\mathrm{Cyr}^{-1}$, 0.02 $^{\mathrm{o}}\mathrm{Cyr}^{-1}$, and 0.06 $^{\mathrm{o}}\mathrm{Cyr}^{-1}$, respectively.

Both Gaussian parameters for the Permafrost Bomb result in a series of permafrost system tipping in the 350 year time span. Each consecutive tipping increases in frequency and decreases in magnitude. When the ground temperature spikes, the ground carbon depletes to 0 kgm^2, at which point the ground temperature decreases to the atmospheric temperatue value. The carbon content then increases until the next tipping event. The tipping in the system with a $\mathrm{T_c}$ of 70$^{\mathrm{o}}\mathrm{C}$ is more drastic, with maximum ground temperature reaching 120$^{\mathrm{o}}\mathrm{C}$ compared to 60$^{\mathrm{o}}\mathrm{C}$ in the system with a $\mathrm{T_c}$ of 40$^{\mathrm{o}}\mathrm{C}$. Additionally, tipping of the 70$^{\mathrm{o}}\mathrm{C}$ $\mathrm{T_c}$ system occurs at a lower rate of atmospheric temperature change. In fact, the 70$^{\mathrm{o}}\mathrm{C}$ $\mathrm{T_c}$ system exhibits tipping even when v is set to 0$^{\mathrm{o}}\mathrm{Cyr}^{-1}$. Lastly, the recovery from peak temperatures to atmospheric temperature is more rapid in the 70$^{\mathrm{o}}\mathrm{C}$ Tc system than the 40$^{\mathrm{o}}\mathrm{C}$ $\mathrm{T_c}$ system.

Permafrost Bomb results, from both $\mathrm{T_c}$ of 70$^{\mathrm{o}}\mathrm{C}$ and a $\mathrm{T_c}$ of 40$^{\mathrm{o}}\mathrm{C}$, differ greatly from the Compost Bomb Instability results in Fig. 2.1 and Fig. 2.2. Firstly, the Compost Bomb Instability model for peatlands has only one major tipping point over the 350 year time

scale while, the Permafrost Bomb model shows a series of tipping points in the permafrost system. Secondly, the tipping of the Compost Bomb Instability occurs at a much higher rate of atmospheric temperature change than that of the Permafrost Bomb. For the Compost Bomb, the threshold rate is $0.11^{o}\mathrm{Cyr}^{-1}$ while in the $40^{o}\mathrm{C}$ $\mathrm{T_c}$ Permafrost Bomb, the threshold rate is $0.02^{o}\mathrm{Cyr}^{-1}$. Additionally, the tipping of the Compost Bomb Instability is more drastic than either Permafrost Bomb experiments, the ground temperature reaching $160^{o}\mathrm{C}$. Lastly, the shape of the tipping point between the Compost Bomb Instabity model is very sharp, as opposed to that in the $40^{o}\mathrm{C}$ $\mathrm{T_c}$ Permafrost Bomb model, where the peaks flatten after the maximum temperature is reached and before the temperature decreases. The $70^{o}\mathrm{C}$ $\mathrm{T_c}$ Permafrost Bomb model has peaks that are sharper than those of the $40^{o}\mathrm{C}$ $\mathrm{T_c}$ Permafrost Bomb model but, not as sharp as in the Compost Bomb Instability model.

2.3 Discussion

2.3.1 Negative Feedback from Microbial Decomposition

A Gaussian representation of the decomposition rates within permafrost leads to the both positive and negative feedback relationship between decomposition rate and ground temperature through internal heat production. The series of system tipping events from the Permafrost Bomb model is reflective of the greater increase of decomposition rate with temperature at low temperatures compared to the exponential used in the Compost Bomb Instability model (Fig. 2.5 and Fig. 2.7). The change in temperature peak shape very sharp in the Compost Bomb Instability model to flattening out in the $40^{o}\mathrm{C}$ $\mathrm{T_c}$ Per-

mafrost Bomb model is a result of the negative feedback between decomposition rate and ground temperature at high temperatures, introduced in the Permafrost Bomb. When the ground temperature returns to the atmospheric temperature, the permafrost carbon reservoir restocks until the next tipping. As the atmospheric temperature increases, less carbon storage is required to set off a tipping scenario, exhibited by the increase in frequency of system tipping through time. Increase in tipping frequency allows less time for the carbon stock to grow, causing the amplitude of system tipping to decrease with successive tipping events. Eventually, the carbon decomposes at an equal or greater rate than it is stored due to high atmospheric temperature, meaning that the carbon content stays at 0 kgm^{-2} and there are no more tipping events observed.

The Permafrost Bomb model with a $\mathrm{T_c}$ of 40$^{\mathrm{o}}\mathrm{C}$ seems more realistic than that with a $\mathrm{T_c}$ of 70$^{\mathrm{o}}\mathrm{C}$. This is based on the fact that the 70$^{\mathrm{o}}\mathrm{C}$ $\mathrm{T_c}$ model showed system tipping when v was 0$^{\mathrm{o}}\mathrm{Cyr}^{-1}$, meaning that atmospheric temperature would consistently be at -3$^{\mathrm{o}}\mathrm{C}$. Based on observation of the majority of permafrost maintaining carbon storage since the LGM, while average temperature values having stayed below 0$^{\mathrm{o}}\mathrm{C}$, the 70$^{\mathrm{o}}\mathrm{C}$ $\mathrm{T_c}$ model can not be accurate (Schuur et al., 2008). Decomposition does occur when the ground temperature is under 0$^{\mathrm{o}}\mathrm{C}$ but, this decomposition rate is very low compared to that occurring during system tipping (Mikan et al., 2002). In addition to not resulting in system tipping below a v value of 0.02$^{\mathrm{o}}\mathrm{Cyr}^{-1}$, the Gaussian $\mathrm{T_c}$ and decomposition rate maximum for the 40$^{\mathrm{o}}\mathrm{C}$ $\mathrm{T_c}$ model was based on data from Pietikainen et al., 2004. Therefore, a Gaussian function representation of permafrost decomposition rates, given in Eq. 2.5, with parameters similar to a $\mathrm{T_c}$ of 40$^{\mathrm{o}}\mathrm{C}$, a of 7, and b of 0.012 would be representative of the permafrost system in the Permafrost Bomb model.

2.3.2 Shortcomings

While the decomposition rate function for the Permafrost Bomb model has been better constrained, there remain shortcomings of the model. The Gaussian function with a $\mathrm{T_c}$ of 40$^{\mathrm{o}}$C, a of 7, and b of 0.012 for parameters, is more realistic than the previously proposed exponential decomposition rate functions and the function tested with a $\mathrm{T_c}$ of 70$^{\mathrm{o}}$C but, it is still only an estimate. Decomposition rate lab analysis should be done on specifically permafrost soils for temperatures ranging up to 60$^{\mathrm{o}}$C, at least, to fully constrain the decomposition rate dependence on ground temperature. An additional fault of the Permafrost Bomb model is that the thermal properties used were the same as those in the Compost Bomb Instability model. Thermal conductivity, k, and heat capacity, μ, however, differ between permafrost and peatlands (Jansson and Karlberg, 2001).

The annual contribution of carbon to the ground reservoir from litter fall was not changed from the Compost Bomb Instability model for peatlands to the Permafrost Bomb model. To continue with this simplified model for permafrost, this litter fall amount should be refined to a permafrost specific value. To make a more accurate model for permafrost, the litter fall should be a temperature dependent function (DeConto et al., 2012). This is because, as atmospheric temperature increases, plant activity also increases so, more organic carbon will be deposited into the ground (DeConto et al., 2012). This feedback was not represented in either the Compost Bomb Instability or Permafrost Bomb model.

2.3.3 Paleocene-Eocene Thermal Maximum

The negative feedback between ground temperature and decomposition rates at higher temperatures may offer support to the Paleocene-Eocene Thermal Maximum (PETM) hyperthermals permafrost hypothesis, presented in DeConto et al., 2012. DeConto et al., 2012 hypothesized that permafrost thaw amplified effects of solar amplification through positive system feedbacks, resulting in the hyperthermals (DeConto et al., 2012). The hyperthermal events were a series of six rapid peaks in atmospheric temperature and carbon content over the course of about two million years following the PETM (Laurentano et al., 2015). Each successive hyperthermal event decreased in amplitude (DeConto et al., 2012). Without considering other climate system feedbacks in the Permafrost Bomb, the same pattern of rapid tipping, followed by rapid recovery, and decreasing amplitude of successive tipping events was observed.

The rapid recovery from each hyperthermal has been explained with the negative feedback between atmospheric temperature and silicate weathering rates and also vegetation draw down (DeConto et al., 2012). The switch to a negative feedback between decomposition rates and ground temperature at high temperatures further supports the practicality of permafrost system tipping and recover involvement in the post PETM hyperthermals. While the time scale of tipping events observed from the Permafrost Bomb and the hyperthermal events varies greatly, this can be explained by the fact that the Permafrost Bomb model was not modeling the precise atmospheric temperature forcing occurring after the PETM. The Permafrost Bomb was simulating a constant increase in atmospheric temperature, while after the PETM, the atmospheric temperature tempera-

tures were being driven by orbital climate forcings so, the temperature not consistently increasing or decreasing during the time span of the hyperthermals (DeConto et al., 2012).

2.3.4 Conclusion

The Permafrost Bomb adaption from the Wieczorek et al., 2010 Compost Bomb Instability model for peatlands considers a Gaussian function for microbial decomposition rates within the ground rather than an exponential function, as in the Compost Bomb Instability. The result is a series of system tipping points which quickly recover to the baseline ground temperature and have decreasing successive amplitude and chage in peak shape. This pattern resembles that of the post PETM hyperthermals, supporting previous hypothesis of permafrost system impact on the behavior of the hyperthermals. The Permafrost Bomb model was therefore informative to the long term patterns of the permafrost system resulting from the decomposition rate ground temperature feedback.

The Permafrost Bomb model could be improved with respiration lab measurements at of carbon rich permafrost soil at higher temperatures to refine the estimated Gaussian decomposition function, $r(T) = \frac{7}{\sqrt{2\pi}} e^{\frac{-0.012}{2}(T-40)^2}\ \mathrm{kgC kgC^{-1} yr^{-1}}$. Additional data analysis and measurements can be made to determine the thermal properties, thermal conductivity and heat capacity, and temperature dependent litter fall function representative of permafrost. The focus of the Permafrost Bomb model was on the relation between ground temperature and decomposition rate but, ultimately, a complete permafrost system model would include the feedback between the permafrost system and atmospheric climate conditions.

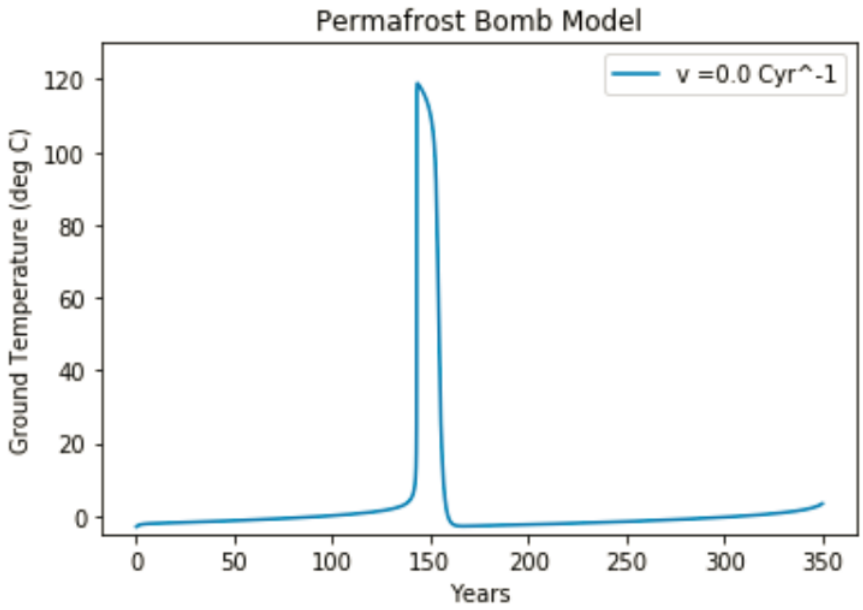

(a) Ground temperature results for $v = 0.0^{\circ}\mathrm{Cyr}^{-1}$.

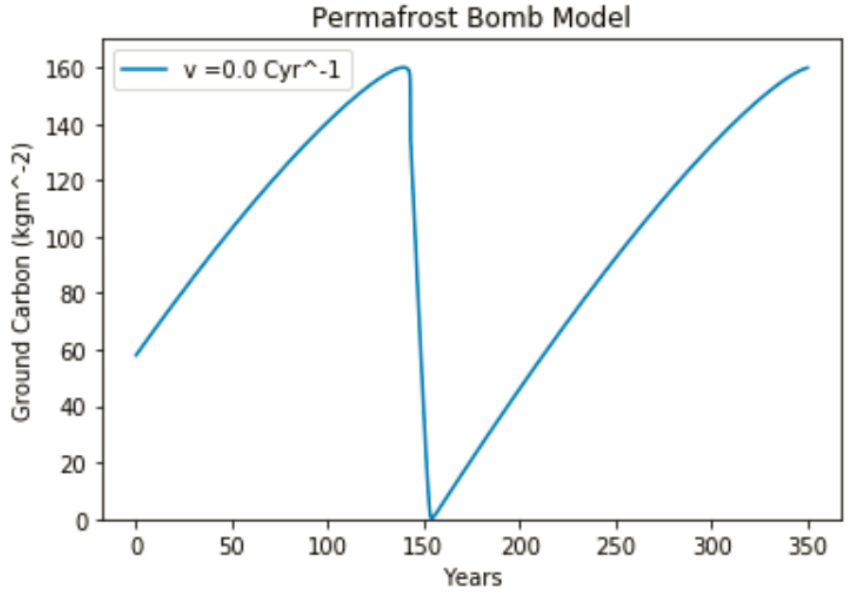

(b) Ground carbon density results for $v = 0.0^{\circ}\mathrm{Cyr}^{-1}$.

Figure 2.9: Permafrost Bomb results for ground temperature and carbon density for $v = 0.0^{\circ}\mathrm{Cyr}^{-1}$, when Gaussian parameters are $\mathrm{T_c}$ = 70°C, $a = 11$, and $b = 0.003$.

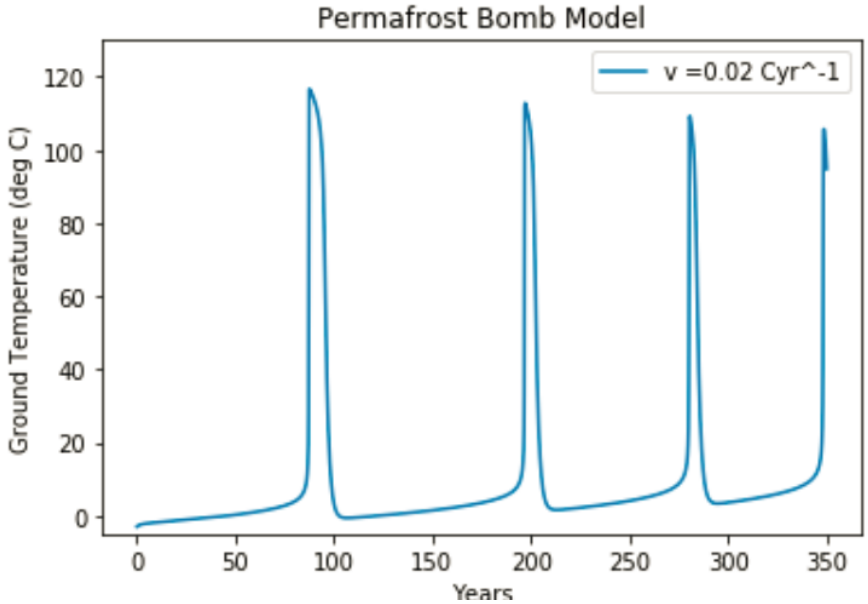

(a) Ground temperature results for $v = 0.02^{\circ}\mathrm{Cyr}^{-1}$.

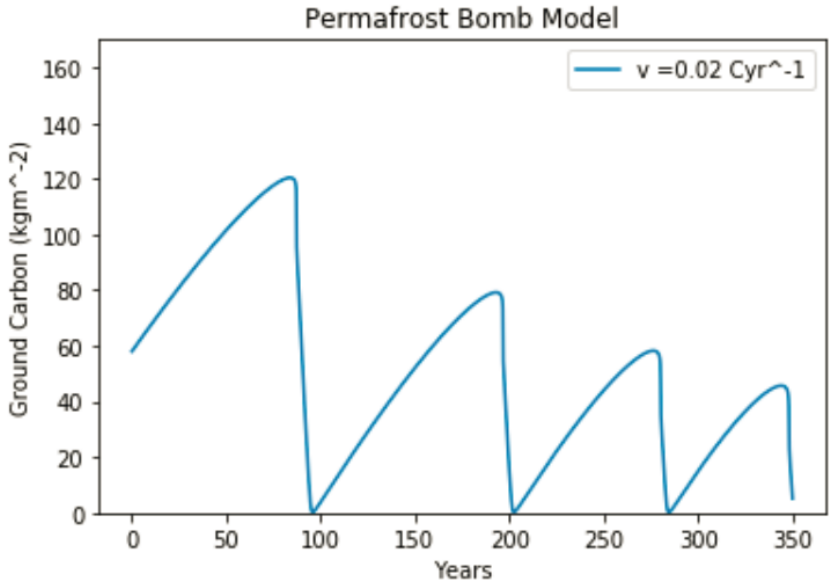

(b) Ground carbon density results for $v = 0.02^{\circ}\mathrm{Cyr}^{-1}$.

Figure 2.10: Permafrost Bomb results for ground temperature and carbon density for $v = 0.02^{\circ}\mathrm{Cyr}^{-1}$, when Gaussian parameters are $\mathrm{T_c} = 70^{\circ}\mathrm{C}$, $a = 11$, and $b = 0.003$.

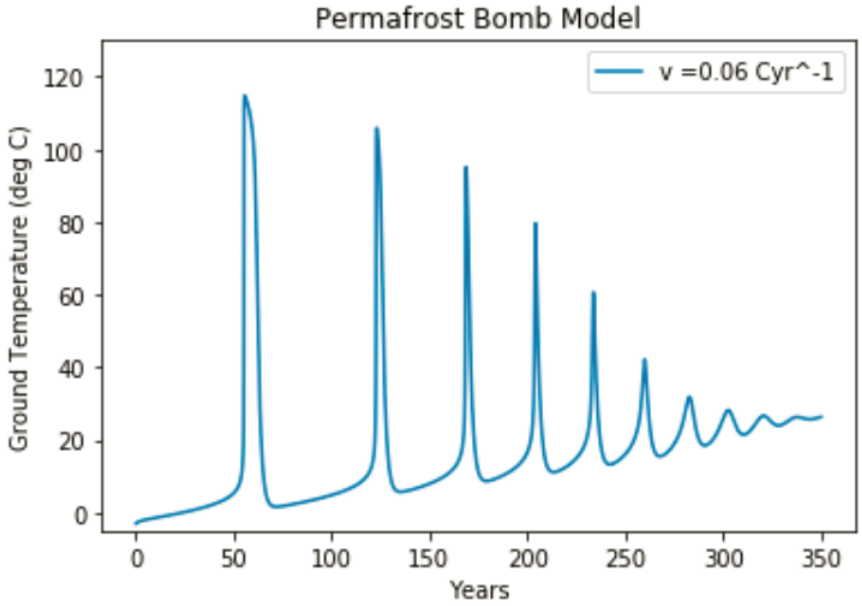

(a) Ground temperature results for $v = 0.06^{\circ}\mathrm{Cyr}^{-1}$.

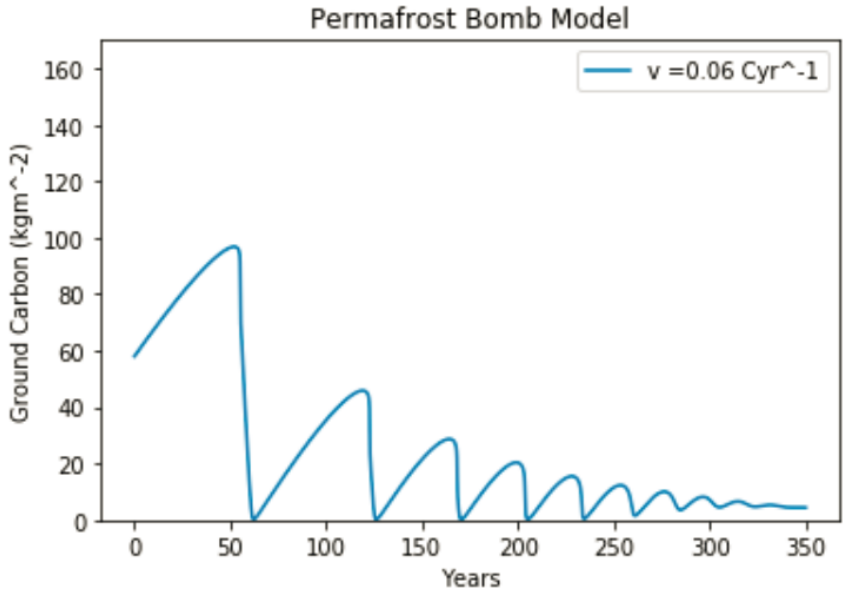

(b) Ground carbon density results for $v = 0.06^{\circ}\mathrm{Cyr}^{-1}$.

Figure 2.11: Permafrost Bomb results for ground temperature and carbon density for $v = 0.06^{\circ}\mathrm{Cyr}^{-1}$, when Gaussian parameters are $\mathrm{T_c}$ = 70°C, $a = 11$, and $b = 0.003$.

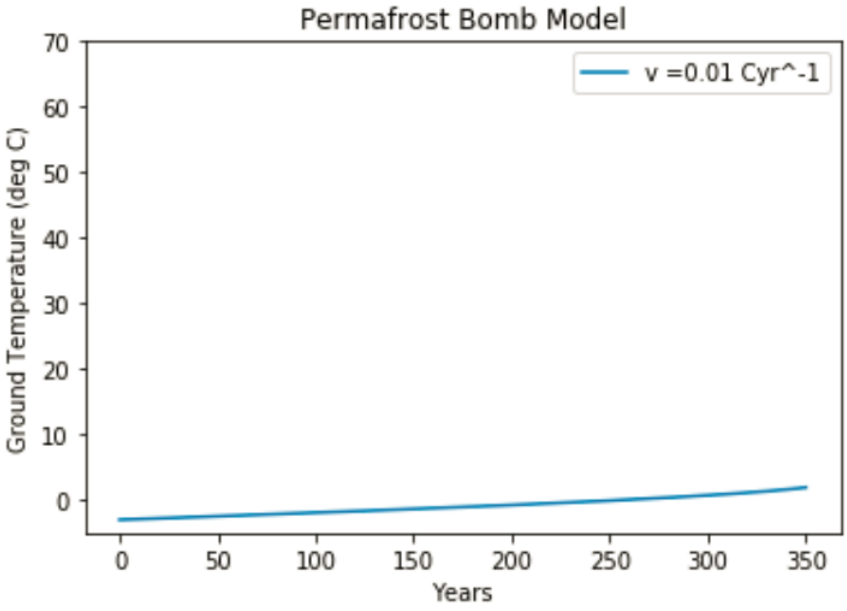

(a) Ground temperature results for $v = 0.01^{\circ}\mathrm{Cyr}^{-1}$.

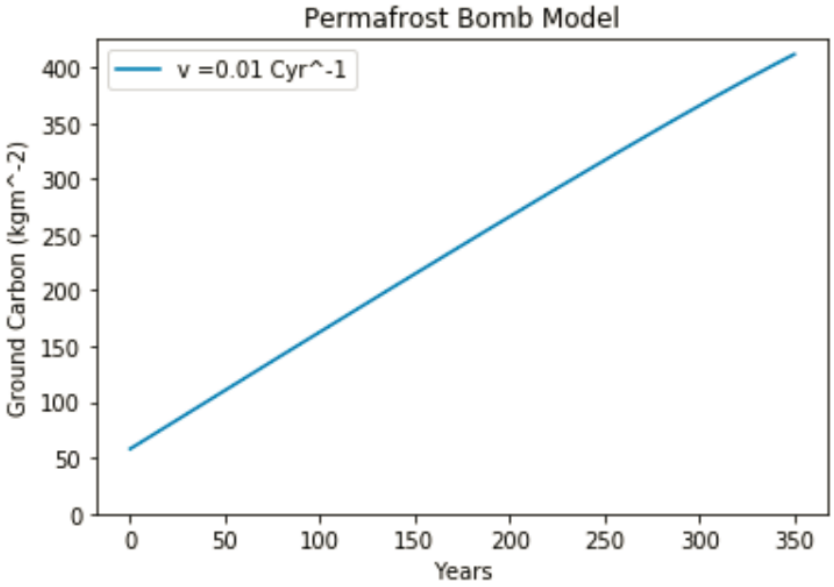

(b) Ground carbon density results for $v = 0.01^{\circ}\mathrm{Cyr}^{-1}$.

Figure 2.12: Permafrost Bomb results for ground temperature and carbon density for $v = 0.01^{\circ}\mathrm{Cyr}^{-1}$, when Gaussian parameters are $\mathrm{T_c} = 40^{\circ}\mathrm{C}$, $a = 7$, and $b = 0.012$.

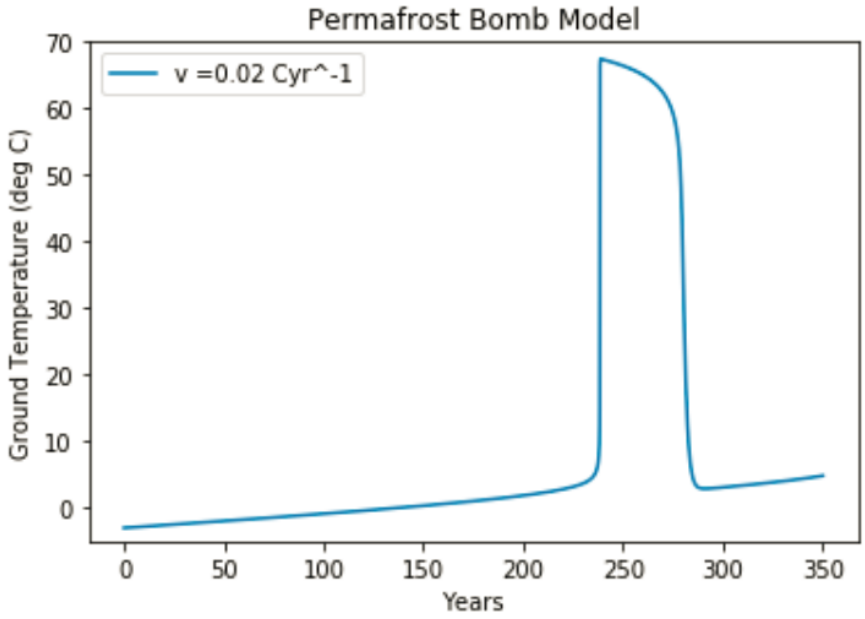

(a) Ground temperature results for $v = 0.02^{\circ}\mathrm{Cyr}^{-1}$.

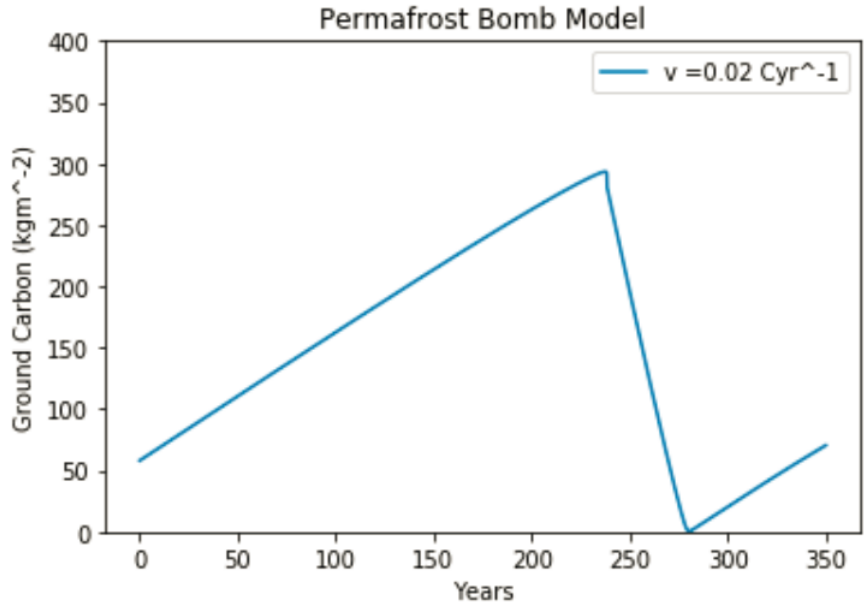

(b) Ground carbon density results for $v = 0.02^{\circ}\mathrm{Cyr}^{-1}$.

Figure 2.13: Permafrost Bomb results for ground temperature and carbon density for $v = 0.02^{\circ}\mathrm{Cyr}^{-1}$, when Gaussian parameters are $\mathrm{T_c} = 40^{\circ}\mathrm{C}$, $a = 7$, and $b = 0.012$.

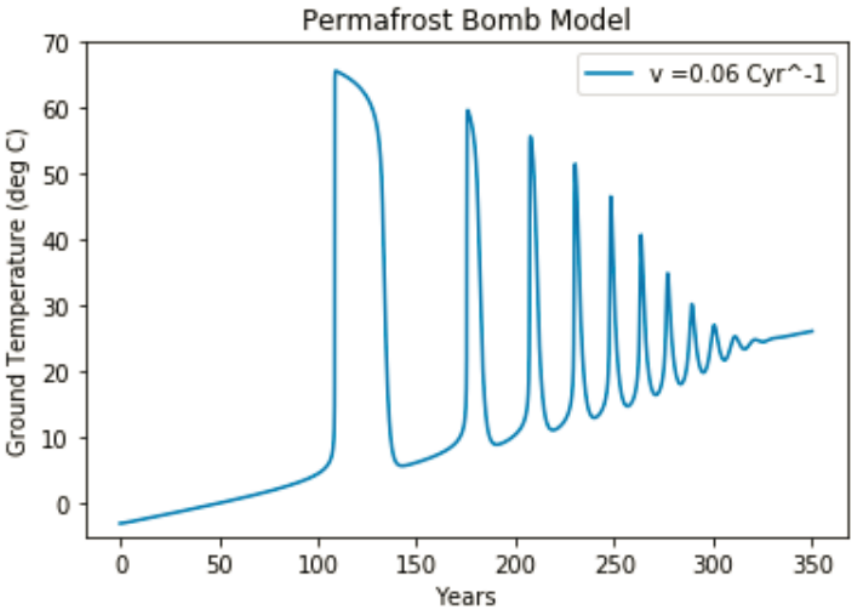

(a) Ground temperature results for $v = 0.06^{\circ}\mathrm{Cyr}^{-1}$.

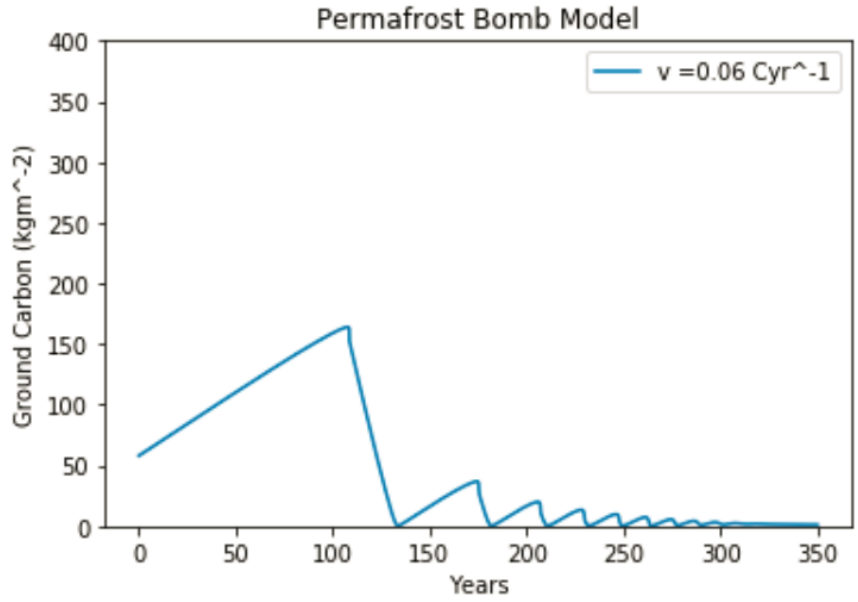

(b) Ground carbon density results for $v = 0.06^{\circ}\mathrm{Cyr}^{-1}$.

Figure 2.14: Permafrost Bomb results for ground temperature and carbon density for $v = 0.06^{\circ}\mathrm{Cyr}^{-1}$, when Gaussian parameters are $\mathrm{T_c}$ = 40°C, $a = 7$, and $b = 0.012$.

Chapter 3

Thermal Properties of Permafrost

3.1 Background and Methods

3.1.1 Thermal Diffusivity in Permafrost Column

The temperature profile of permafrost is largely dictated by its thermal properties; thermal conductivity and specific heat capacity (Osterkamp and Burn, 2003). Thermal conductivity defines a materials ability to conduct heat and specific heat capacity is the heat required to change a materials temperature by one degree kelvin (Frob, 2011). The thermal conductivity to heat capacity ratio is termed thermal diffusivity and measures the rate of heat transfer through a material (Frob, 2011). Eq. 3.1 defines thermal diffusivity in terms of thermal conductivity, k, and specific heat capacity, c_p (Frob, 2011). The heat transfer equation, Eq. 3.2, describes how permafrost temperature at a specific depth changes in response to the heat difference between surrounding depths (Frob, 2011).

$$d_h = \frac{k}{C_p} \tag{3.1}$$

$$\frac{\partial T}{\partial t} = d_h \frac{\partial^2}{\partial z^2} T(z,t) \tag{3.2}$$

Both thermal conductivity and specific heat capacity are recognized to be dependent on permafrost composition (Jansson and Karlberg, 2001). In addition to the general permafrost geology and lithology, the precise permafrost composition includes water content, ice content, and air content (Roth and Boike, 2001). Due to local landscape and temperature variation, the latter three components change through time and, as a result, so do the permafrost thermal properties (Jansson and Karlberg, 2001). While a variety of measurements have been made to define these thermal properties, how they may change through time and depth in permafrost has not been explicitly described.

The specific heat capacity can be calculated by summing the heat capacity contributions from each mass component but, the complexity of the changing permafrost composition raises difficulty with this calculation (Jansson and Karlberg, 2001). Thermal conductivity is even more variable, sensitive to vegetation cover, water movement, and other parameters challenging to quantify (Frob, 2011). Therefore, thermal diffusivity is an accessible and informative measure of the permafrost thermal properties, as it considers the change in k and c_p in one term. The purpose of this experiment is to determine how thermal diffusivity varies through time and depth at a Kapp Linné, Svalbard borehole by analyzing ground temperature data.

3.1.2 Estimation of Thermal Diffusivity from Temperature Profile

Borehole data and information for Kapp Linné 1 was retrieved from the Global Terrestrial Network for Permafrost database. The entire borehole is through bedrock and, collected

temperature readings every 6 hrs from September 2008 through April 2015 (Christiansen, 2016). The temperature points are taken at precise finite depths so, the permafrost will be treated as a series of finite ground layers in analysis. A Monte Carlo based method of thermal diffusivity, d_h, calculation is used. Temperature values for a given layer of permafrost are modeled using an estimated d_h and temperature data from the bounding layers in the heat transfer equation. The heat transfer equation for a finite i_{th} layer of permafrost is given in Eq. 3.3 (Recktenwald, 2011).

$$\frac{\partial T}{\partial t} = d_h \frac{T_{i+1} - 2T_i + T_{i-1}}{2\Delta z^2} \tag{3.3}$$

The modeled and collected temperature data for the i_{th} layer is compared over a 30 day time-frame and the root mean square error is calculated. Fig. 3.1 shows an example of the modeled temperature for a permafrost layer compared to the true data for the i_{th} layer and bounding layers. A 30 day test window was chosen to include enough data points for informative root mean square error comparison but, a small enough such that thermal diffusivity will not change significantly within the test period. This process is repeated for the same 30 day window for a range of d_h estimations. Fig. 3.2 compares the estimated d_h used to the corresponding root mean square error for a single permafrost depth and time window. The d_h value that results in the lowest error is recorded as the accurate value for that layer at that time step. An example of the root mean square error minimum is clearly seen in Fig. 3.2. This procedure was replicated for the same layer of permafrost over the entire time series of available temperature data, giving the d_h values through time. 30 day window start days were separated by 15 days.

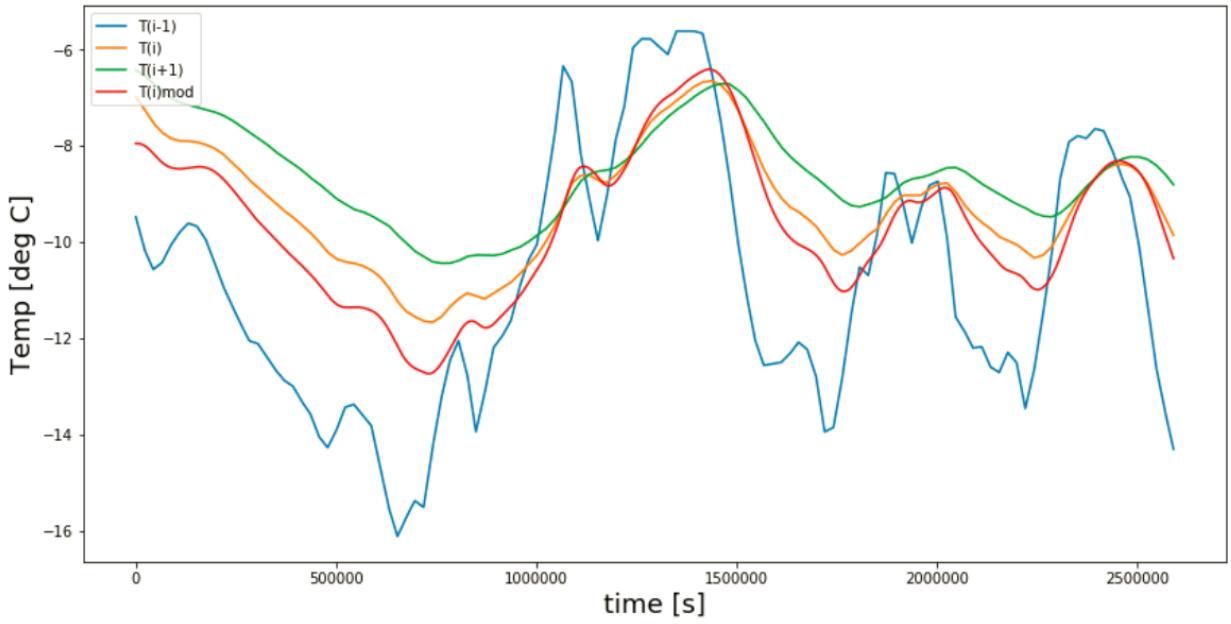

Figure 3.1: Graph of temperature data for three consecutive permafrost depths as well as the modeled temperature data for the middle layer. Example where, estimated d_h is 5.0×10^{-7} $\mathrm{m}^2\,\mathrm{s}^{-1}$, the modeled layer is permafrost depth 0.5m, and the window start day is day 800.

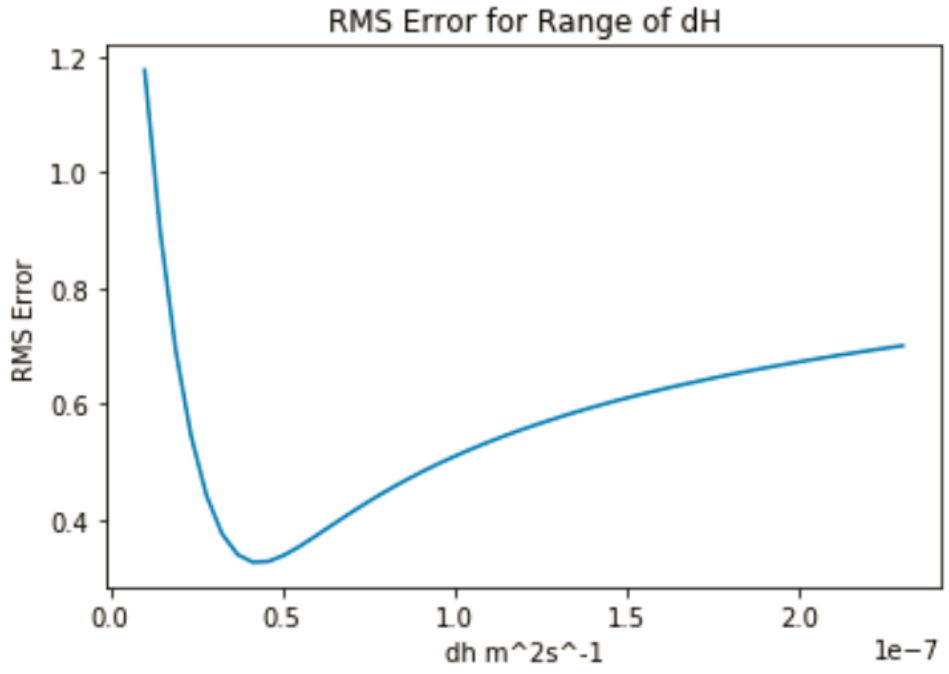

Figure 3.2: Graph of root mean square error against estimated d_h for permafrost depth 0.5m and a 30 day time window starting on day 800.

3.1.3 Method Limitations

Error in the thermal diffusivity values determined with this method do exist. Firstly, the rate of temperature change equations, Eq. 3.3, only consider the flux of heat from surrounding permafrost layers. In permafrost, there is also heat flux from the latent heat of water phase transitions and heat produced by microbial decomposition (Jansson and Karlberg, 2001). Therefore, the results are representative of the apparent d_h rather than the true d_h. The Kapp Linné borehole is completely bedrock so, impact from microbial decomposition is nonexistent. Latent heat, however, definitely contributes to the Kapp Linné borehole profile. This is important to consider in the evaluation of results as, drastic change in apparent d_h may be representative of change in latent heat contribution rather than a change in the material thermal properties. Secondly, there is uncertainty in the thermal diffusivity values due to the fact that the range of d_h values analyzed is finite. The difference between tested d_h is $2.0\times10^{-7}\ \mathrm{m^2\,s^{-1}}$. This will result in the discretization of results, where many calculated d_h values may flat line at the same value. Lastly, the test window for determination of most accurate d_h value means that the d_h values reported for a given window start day are representative of the best fit over the following 30 days, not the specific d_h on that day.

3.2 Kapp Linné 1 d_h Results

Temperature data from Kapp Linné 1 was analyzed for thermal diffusivity values for depths 0.25m, 0.5m, 1m, 1.5m, 2.5m, 3m, 5m, and 10m. Fig. 3.3 shows the ground temperature data for these 8 layers from September 2008 through April 2015. Table 3.1 sum-

marizes the thermal diffusivity results by maximum and minimum value for each depth. In addition to the calculation of thermal diffusivity through time and depth, the thawed depth of the borehole was calculated. This was done by declaring the maximum depth, from the surface, that was greater or equal to $0^{o}\mathrm{C}$ to be thawed. The thawed depth was calculated at every time interval of the Kapp Linné 1 data set. The maximum thaw depth for a given year is typically around 2.5m and defines the base of the active layer.

Depth (m)	d_h **min** ($\mathrm{m^2\,s^{-1}}$)	d_h **max** ($\mathrm{m^2\,s^{-1}}$)
0.25	1.16 $\times 10^{-8}$	1.10 $\times 10^{-6}$
0.5	2.04 $\times 10^{-7}$	1.16 $\times 10^{-5}$
1.0	4.63 $\times 10^{-7}$	6.26 $\times 10^{-5}$
1.5	1.16 $\times 10^{-7}$	3.47 $\times 10^{-5}$
2.5	2.37 $\times 10^{-7}$	1.11 $\times 10^{-4}$
3.0	2.37 $\times 10^{-7}$	1.11 $\times 10^{-4}$
5.0	1.44 $\times 10^{-7}$	2.16 $\times 10^{-6}$
10.0	2.28 $\times 10^{-6}$	1.0 $\times 10^{-3}$

Table 3.1: Maximum and Minimum d_h Values Calculated for Each Depth.

3.2.1 Depth 0.25m

0.25m is the most shallow borehole depth with temperature data. The temperature ranges, roughly, from -15$^{o}\mathrm{C}$ to 10$^{o}\mathrm{C}$ within every year. This means that 0.25m is within the active layer and thaws and refreezes yearly. The d_h values calculated range between 1.16$\times 10^{-8}$

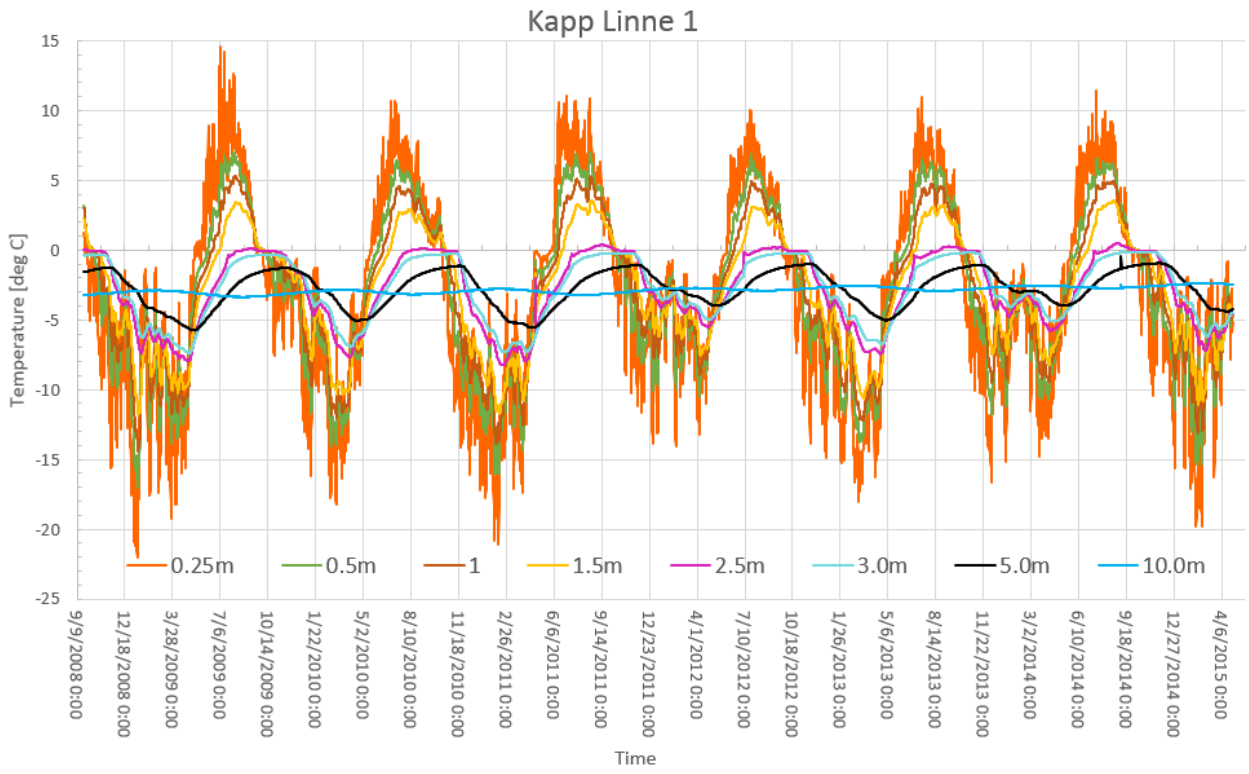

Figure 3.3: Ground temperature data from borehole Kapp Linné 1. Data is from the GTNP database and was originally collected by Hanne Christiansen.

$\mathrm{m^2\,s^{-1}}$ and 1.0×10^{-6} $\mathrm{m^2\,s^{-1}}$. Fig. 3.4 shows the d_h values calculated throughout the entire time series, where the window start day was the starting point of the 30 day d_h value test. The thawed depth at Kapp Linné 1 is also shown in Figure 4. There is clear correlation between d_h and thawed depth presented in Fig. 3.4, as the minimum d_h values occur when the thawed depth rapidly increase from 0m or decreases to 0m. This timing is representative of when the ground is thawing and freezing.

Fig. 3.5 presents the same d_h results from 0.25m but, plots the each year of data on the same x-axis for day of year of window start day. From Fig. 3.4, it can be seen that the pattern of d_h value throughout the year is cyclical, with local minimas, d_h of 1.16×10^{-8} $\mathrm{m^2\,s^{-1}}$, occurring in the spring and fall. The winter tends to have a lower and less erratic

d_h pattern than the summer. The year with winter d_h values closest to the summer d_h trend is 2011.

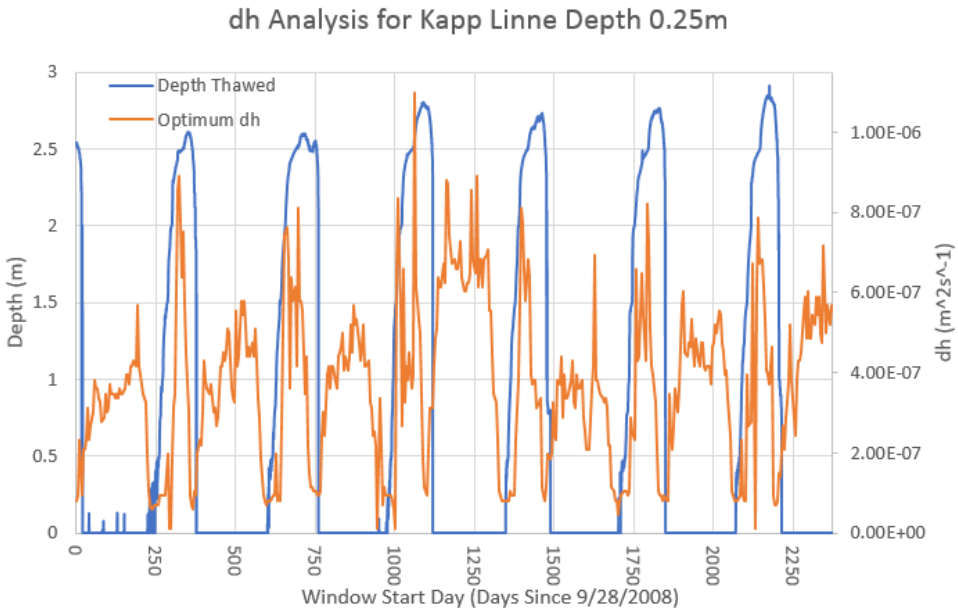

Figure 3.4: Results of thermal diffusivity analysis at 0.25m depth, in blue. In orange, the thawed depth of the Kapp Linné 1 borehole through the same time period.

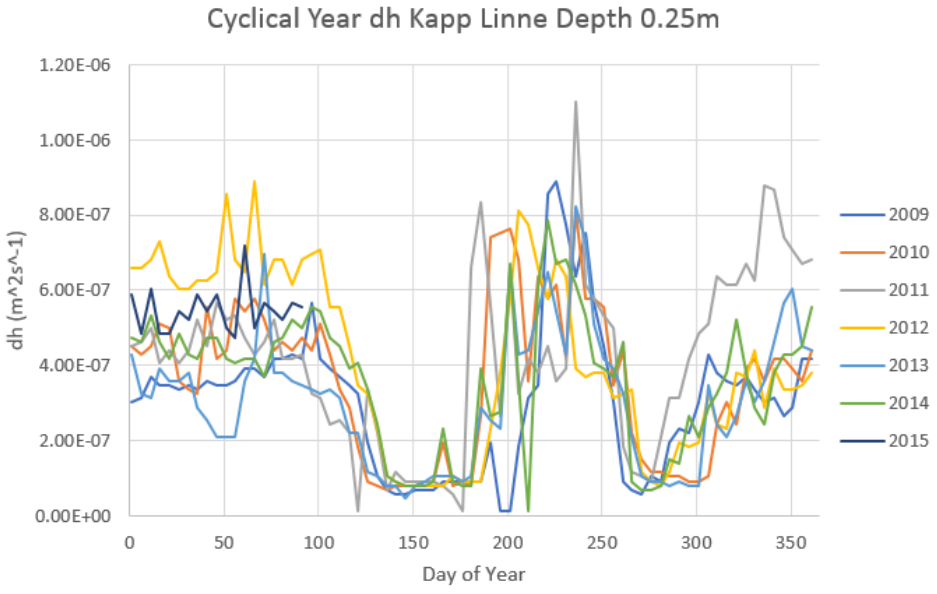

Figure 3.5: Results of thermal diffusivity analysis at 0.25m depth from individual years.

3.2.2 Depth 0.5m

The temperature for 0.5m ranges from -13^{o}C to 6^{o}C within every year. It is well within the active layer. The d_h values calculated range between 2.04$\times 10^{-7}$ $\mathrm{m^2\,s^{-1}}$ and 1.16$\times 10^{-5}$ $\mathrm{m^2\,s^{-1}}$. Fig. 3.6 shows the d_h values calculated throughout the entire time series superimposed with the thawed depth at Kapp Linné 1. The results show very sharp transitions from minimum to maximum values. Maximum values of d_h occur right before the thawed depth rapidly increases from 0m to 2.5m but, drop back towards the minimum d_h value before the thawed depth reached the yearly maximum. This pattern is observed from 2010 onward but, not in 2009. Calculated thermal diffusivity is always at its lowest during the period of thawed permafrost in the summer. Each consecutive year, the fall and winter d_h values increase and become more variable. Fig. 3.7 presents the d_h results from 0.5m plotted by year. This shows the consistency in the patterns described; maximum thermal diffusivity in the spring, minimum in the summer and fall, and low and variable in the winter.

3.2.3 Depth 1.0m

The temperature for 1m ranges from -10^{o}C to 5^{o}C within every year and is within the active layer. The d_h values calculated range between 4.63$\times 10^{-7}$ $\mathrm{m^2\,s^{-1}}$ and 6.26$\times 10^{-5}$ $\mathrm{m^2\,s^{-1}}$. Fig. 3.8 shows the d_h values calculated throughout the entire time series superimposed with the thawed depth at Kapp Linné 1. The results show very sharp transitions from minimum to maximum values. The period of time when the permafrost had a 0m thaw depth is when the maximum d_h were calculated. Most of the the d_h in this time period are

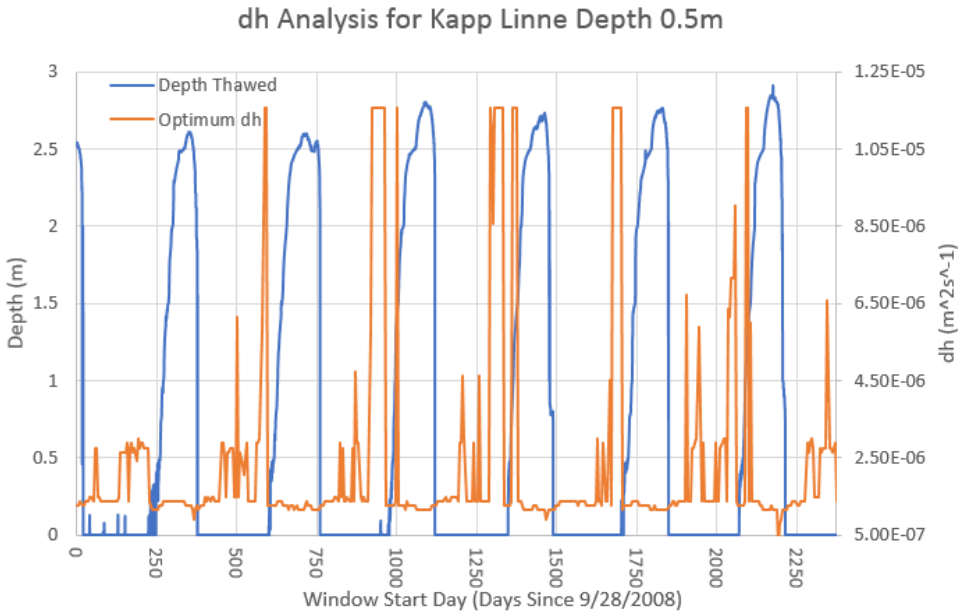

Figure 3.6: Results of thermal diffusivity analysis at 0.5m depth, in blue. In orange, the thawed depth of the Kapp Linné 1 borehole through the same time period.

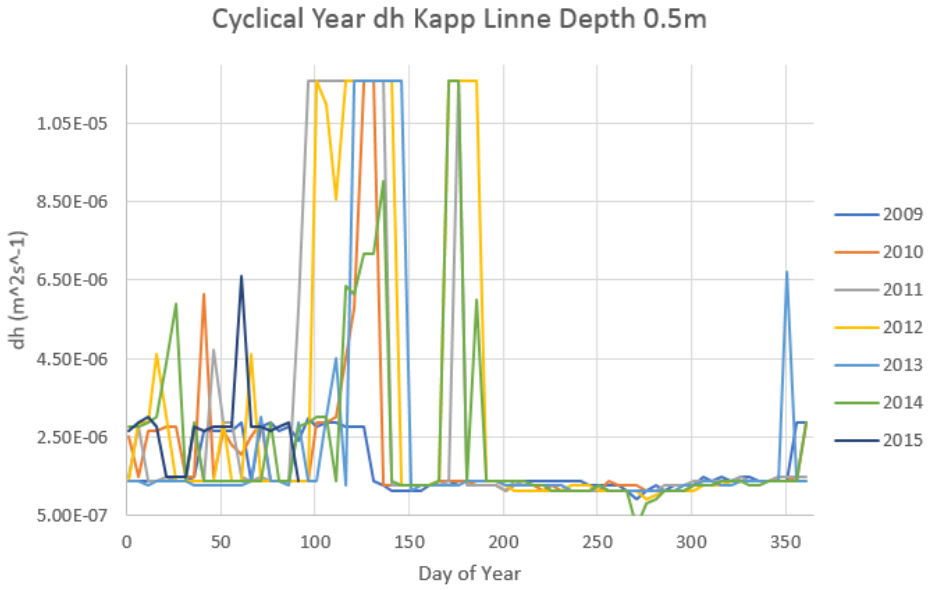

Figure 3.7: Results of thermal diffusivity analysis at 0.5m depth from individual years.

exactly at the maximum of 6.26×10^{-5} $\mathrm{m^2\,s^{-1}}$, which is likely a result of the d_h test value resolution. This period of time has a few low spikes in d_h as well. When the permafrost has the maximum thaw depth, in the summer, the minimum d_h values were calculated.

Fig. 3.9 presents the d_h results from 1m plotted by year.

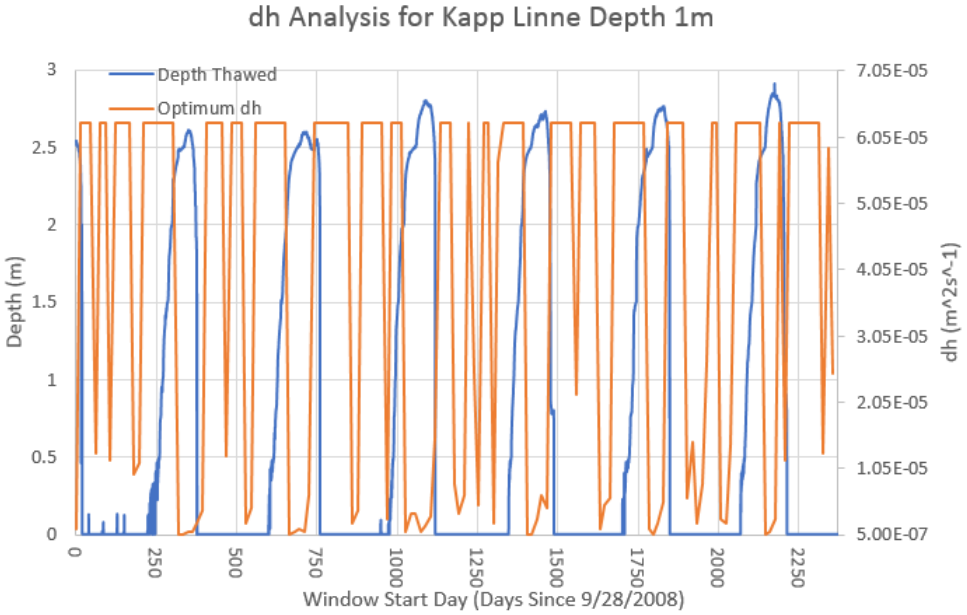

Figure 3.8: Results of thermal diffusivity analysis at 1m depth, in blue. In orange, the thawed depth of the Kapp Linné 1 borehole through the same time period.

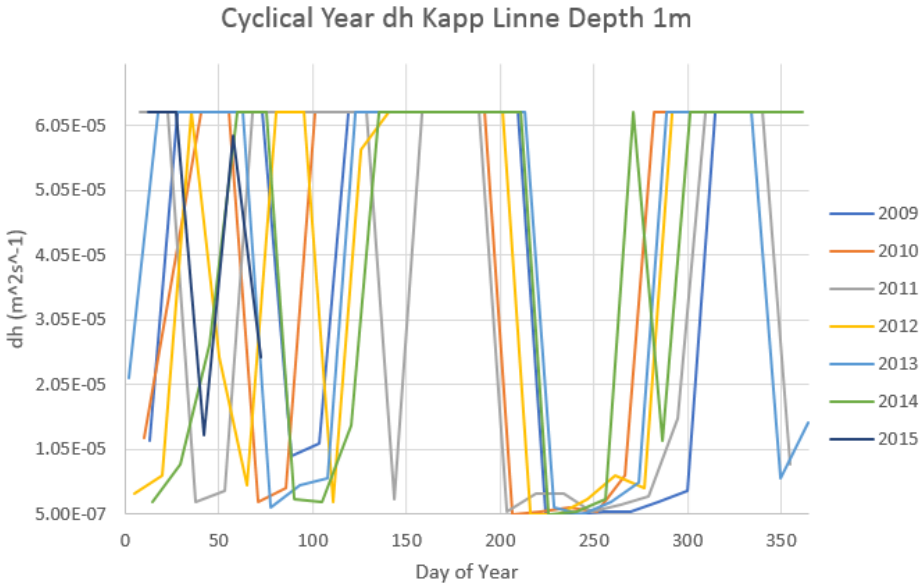

Figure 3.9: Results of thermal diffusivity analysis at 1m depth from individual years.

3.2.4 Depth 1.5m

The temperature for 1.5m ranges from -10°C to 3°C within every year and in the active layer. The d_h values calculated range between 1.16×10^{-7} $\mathrm{m^2\,s^{-1}}$ and 3.47×10^{-5} $\mathrm{m^2\,s^{-1}}$. Fig. 3.10 shows the d_h values calculated throughout the entire time series superimposed with the thawed depth at Kapp Linné 1. The results show very sharp transitions from minimum to maximum values. Maximum d_h was calculated just when the permafrost is beginning to thaw. The only year that this pattern was not observed was 2010. Small peaks are seen both right before and right after the permafrost freezes. Otherwise, the calculated d_h remains low, near minimum value. Fig. 3.11 presents the d_h results from 1.5m plotted by year. This clearly shows precisely when the maximum d_h values are being calculated in the different years. In 2011 the d_h peak to the maximum value was calculated in early spring. In 2012, 2013, and 2014 are years in which the peak was calculated in late spring to early summer. In 2009 and 2013, the peak was calculated in late summer. 2013 is the only year with two large d_h peaks calculated.

3.2.5 Depth 2.5m

The temperature for 2.5m ranges from -10°C to 0°C within every year. The active layer depth throughout the time series is between 2.5m and 3m, meaning that the maximum temperature does get just above 0°C every year. The d_h values calculated range between 2.3×10^{-7} $\mathrm{m^2\,s^{-1}}$ and 1.11×10^{-4} $\mathrm{m^2\,s^{-1}}$. Fig. 3.12 shows the d_h values calculated throughout the entire time series superimposed with the thawed depth at Kapp Linné 1. The results show very sharp transitions from minimum to maximum values. Mostly, maxi-

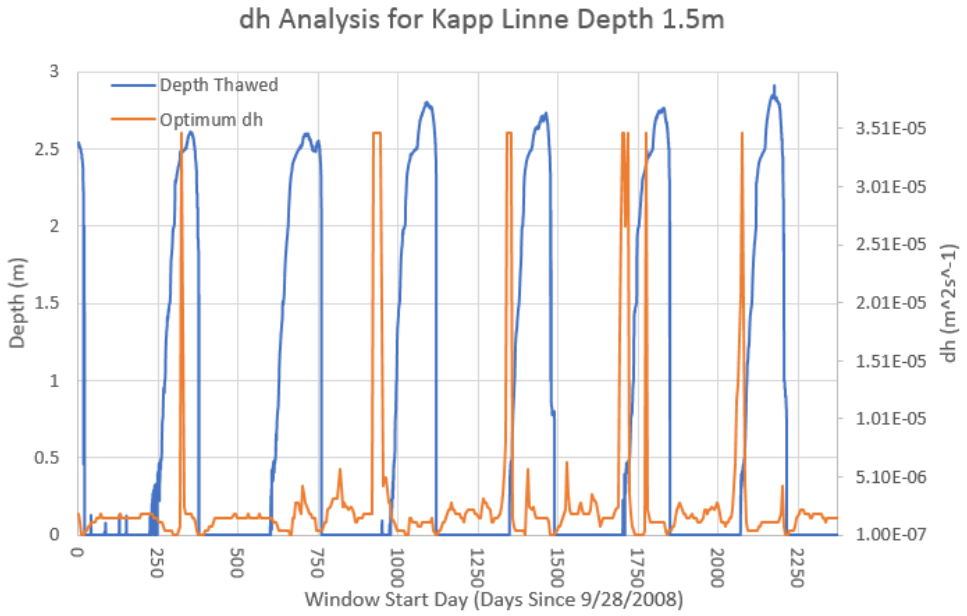

Figure 3.10: Results of thermal diffusivity analysis at 1.5m depth, in blue. In orange, the thawed depth of the Kapp Linné 1 borehole through the same time period.

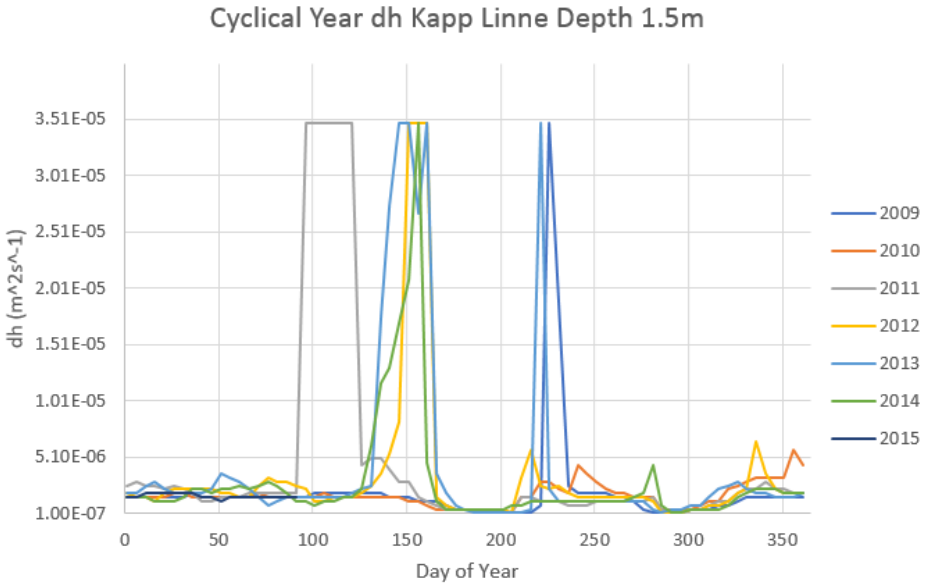

Figure 3.11: Results of thermal diffusivity analysis at 1.5m depth from individual years.

mum d_h was calculated just when the permafrost is most thawed and miniums between thaw periods. There are a few years where d_h peaks occur before the permafrost thaws as well. Fig. 3.13 presents the d_h results from 2.5m plotted by year. Peaks in d_h were

calculated in 2011 in mid-winter, in 2011 and 2014, early spring, in 2012 and 2013, late spring, in 2012, early summer, and in all years, early fall. Generally, more separate peaks have been observed as years have progressed. That is, that there was one peak in 2009 and 2010, three in 2011 and 2012, and two in 2013 and 2014.

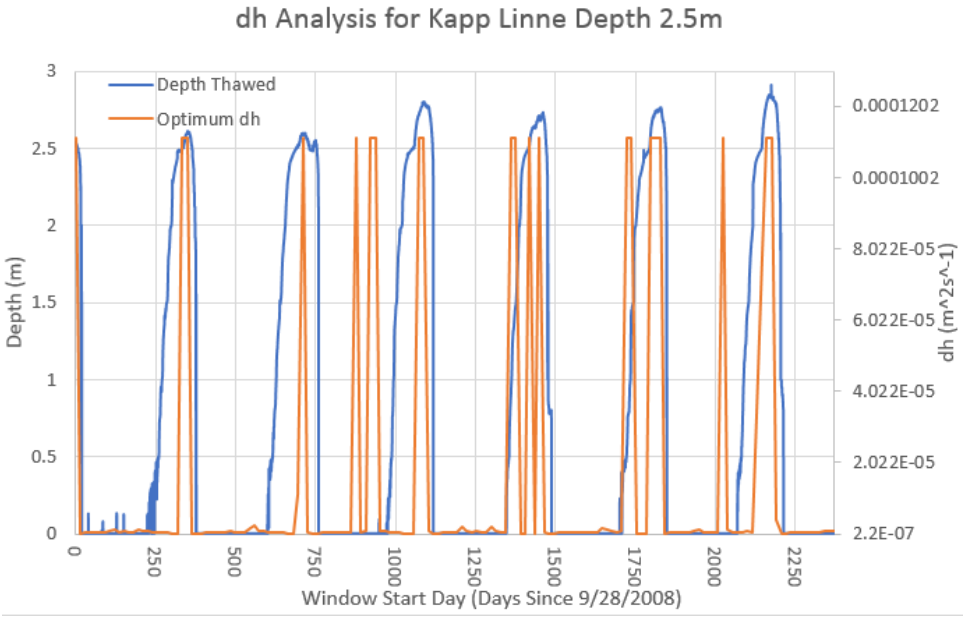

Figure 3.12: Results of thermal diffusivity analysis at 2.5m depth, in blue. In orange, the thawed depth of the Kapp Linné 1 borehole through the same time period.

3.2.6 Depth 3.0m

The temperature for 3m ranges from -6°C to 0°C within every year. The active layer depth never reached 3m in the time series, meaning that the maximum temperature does is never above 0°C. The maximum active layer depth over the time series is 2.8m, occurring in 2014. The d_h values calculated range between 2.3×10^{-7} $\mathrm{m^2\,s^{-1}}$ and 1.11×10^{-4} $\mathrm{m^2\,s^{-1}}$. Fig. 3.14 shows the d_h values calculated throughout the entire time series superimposed with the thawed depth at Kapp Linné 1. The calculated d_h is near the maximum value

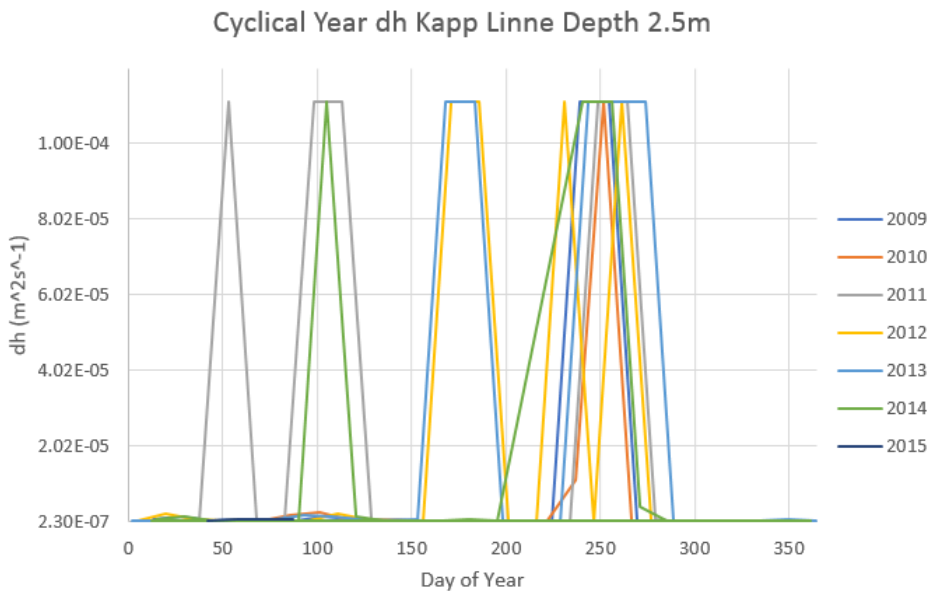

Figure 3.13: Results of thermal diffusivity analysis at 2.5m depth from individual years.

for the majority of the time series. The flat line of repeated 1.11×10^{-4} $\mathrm{m^2\,s^{-1}}$ calculated is signature of the maximum d_h tested. Minimum values regularly are measured after the permafrost has frozen. Fig. 3.15 presents the d_h results from 3m plotted by year. Fig. 3.15 confirms two defined drops in the calculated d_h value, to the minimum, twice a year. These occur in early spring and early to mid fall.

3.2.7 Depth 5.0m

The temperature for 5m ranges from -5°C to -1°C within every year. This depth is below the active layer, remaining frozen year round. The d_h values calculated range between 1.44×10^{-7} $\mathrm{m^2\,s^{-1}}$ and 2.16×10^{-6} $\mathrm{m^2\,s^{-1}}$. Fig. 3.16 shows the d_h values calculated throughout the entire time series superimposed with the thawed depth at Kapp Linné 1. The calculated d_h is around 1.5×10^{-6} $\mathrm{m^2\,s^{-1}}$ for the majority of the time series. Thermal diffusivity begins to decrease when the active layer thaws, reaching the minimum value when

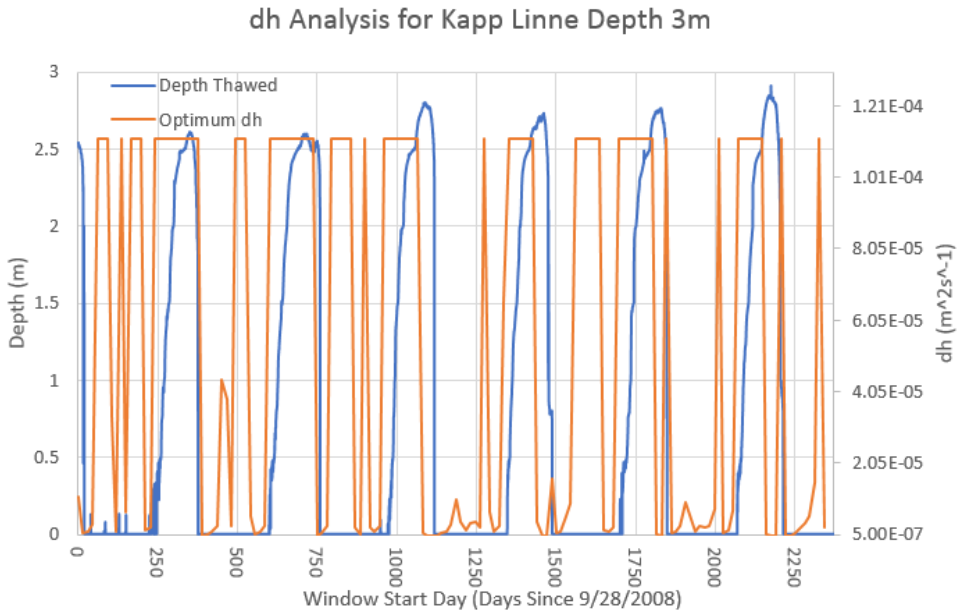

Figure 3.14: Results of thermal diffusivity analysis at 3m depth, in blue. In orange, the thawed depth of the Kapp Linné 1 borehole through the same time period.

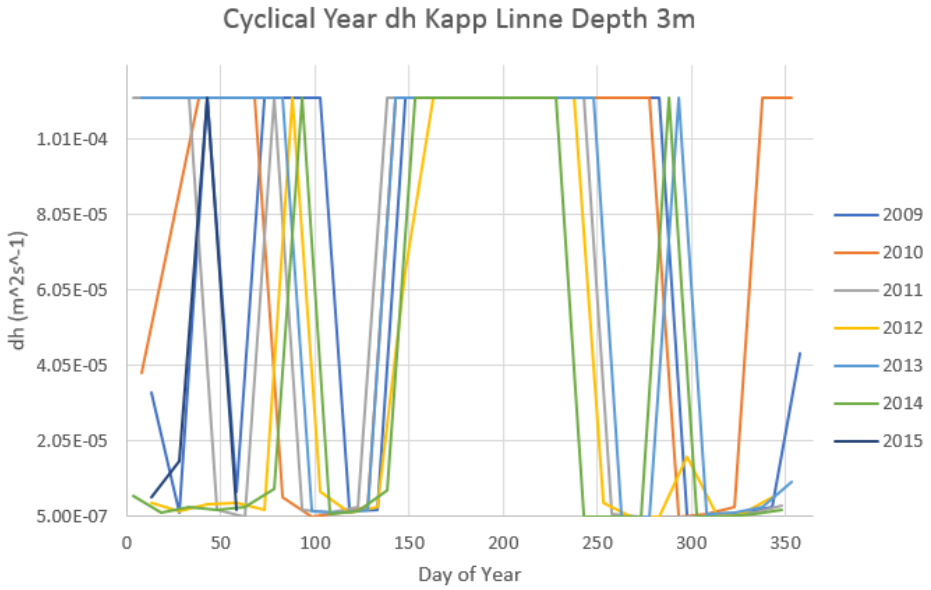

Figure 3.15: Results of thermal diffusivity analysis at 3m depth from individual years.

the permafrost begins to freeze again. Then, the d_h value rapidly peaks to the maximum value right after the permafrost freezes. Fig. 3.17 presents the d_h results from 5m plotted by year. The described pattern of minimum to maximum occurs in late fall.

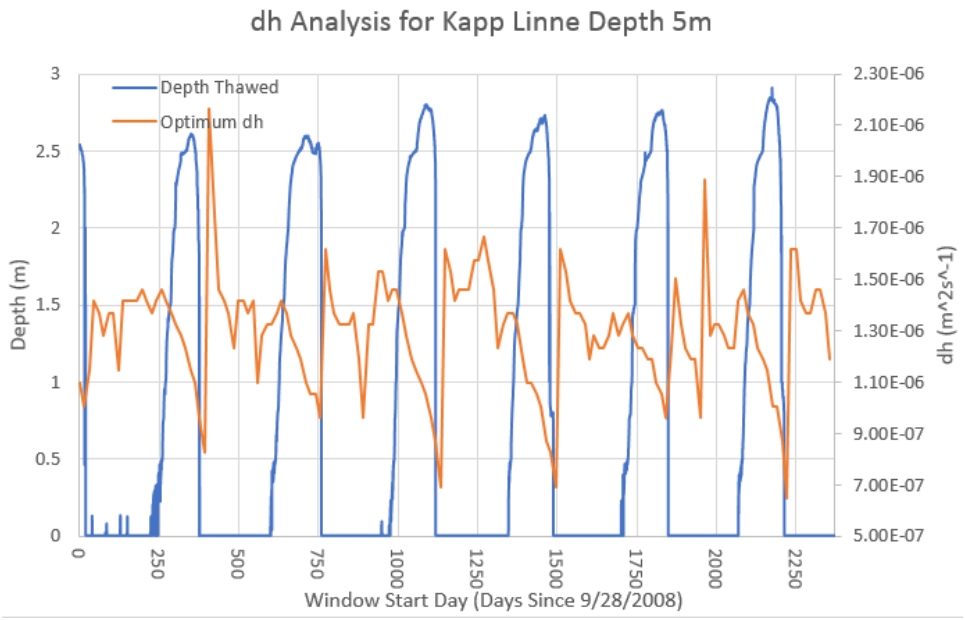

Figure 3.16: Results of thermal diffusivity analysis at 5m depth, in blue. In orange, the thawed depth of the Kapp Linné 1 borehole through the same time period.

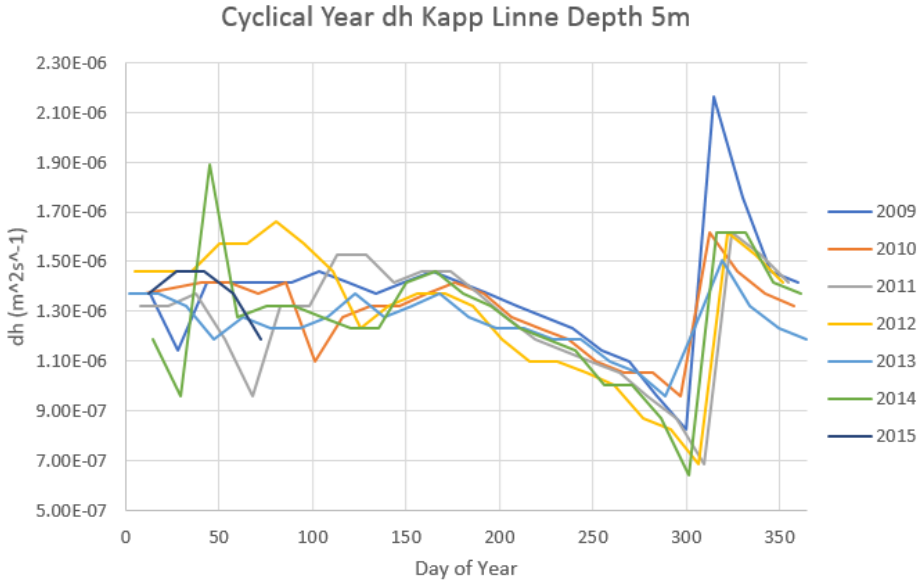

Figure 3.17: Results of thermal diffusivity analysis at 5m depth from individual years.

3.2.8 Depth 10.0m

The temperature for 10m ranges from -3°C to -2°C within every year. This depth is well below the active layer. The d_h values calculated range between 2.28×10^{-7} $\mathrm{m^2\,s^{-1}}$ and

1.0×10^{-3} $\mathrm{m^2\,s^{-1}}$. Fig. 3.18 shows the d_h values calculated throughout the entire time series superimposed with the thawed depth at Kapp Linné 1. Most of the calculated d_h are either exactly 1.0×10^{-3} $\mathrm{m^2\,s^{-1}}$ or exactly 2.28×10^{-7} $\mathrm{m^2\,s^{-1}}$, reflective of the d_h test interval resolution. Fig. 3.19 presents the d_h results from 10m plotted by year. In 2009, the d_h value maintains the minimum value for the entire year. In 2010, the maximum d_h value occurs when the active layer is thawing and immediately returns to the minimum. In each consecutive year, the d_h value reaches the maximum when the active layer is thawed, mid summer, but, remains at the maximum for a longer duration of time. 2011 is unique, as it has two d_h peaks, one when the active layer is thawing and one after the active layer has frozen.

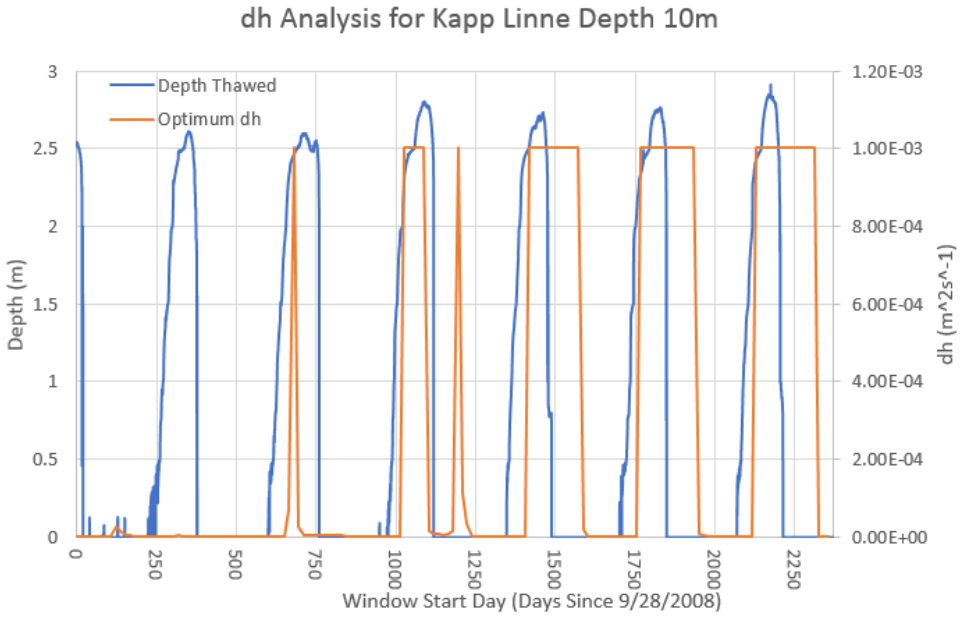

Figure 3.18: Results of thermal diffusivity analysis at 10m depth, in blue. In orange, the thawed depth of the Kapp Linné 1 borehole through the same time period.

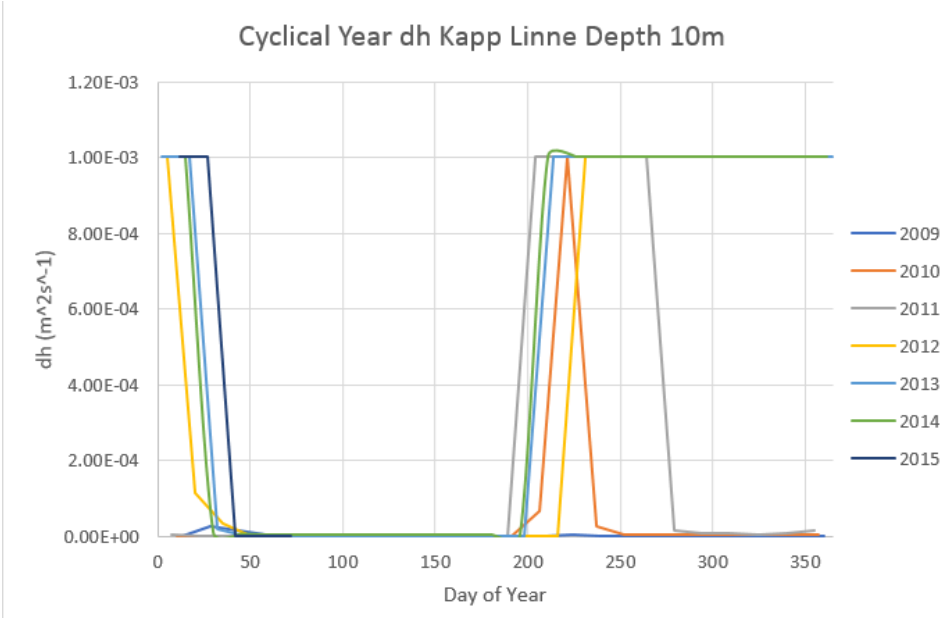

Figure 3.19: Results of thermal diffusivity analysis at 10m depth from individual years.

3.3 Discussion

3.3.1 Effect of Latent Heat

Latent heat is released during phase transition, such as that between ice and water within permafrost. Latent heat will have the largest effect on the permafrost temperature, and therefore calculated d_h, when the temperature is $0^{o}\mathrm{C}$(Romanovsky and Osterkamp, 2000). Latent heat release will impact heat transfer when there is a combination of both ice and water but, not when just either component (Osterkamp and Burn, 2003). Typically, water spatially distributes latent heat and retards the permafrost thermal response, decreasing d_h (Romanovsky and Osterkamp, 2000). At all depths, the change in thermal diffusivity through time has some alignment on the thawing and freezing of the permafrost active layer. This means that the significant changes in calculated thermal diffusivity are a result of latent heat contributing to the layer temperature. The effect, however, is not uni-

form throughout all depths, as some calculated thermal diffusivity values increase during freezing or thawing and others decrease during freezing or thawing.

3.3.2 d_h Variation with Depth

The calculated thermal diffusivity varies greatly between the Kapp Linné depth and even at a single depth throughout the year. The smallest d_h value range was observed at 0.25m and 5m, and the highest at 10m. Between depths, the maximum d_h varies by a factor of 1000. At a single depth, the range of d_h values can vary by a factor of 100 to 1000.

At 0.25m depth, the latent heat effects the thermal diffusivity calculation in the spring, when ground ice thaws, and in the fall, when groundwater freezes. The thermal diffusivity also seems affected by seasonal ground condition as, the values are greater in the summer, when there is no ice, than the winter, when there is no water. The only year that did not have winter d_h values less than that of summer was 2011, which is the year of warm Arctic temperature anomaly due to El Nina, a climate phenomena (Lee, 2012). These patterns suggest a thermal diffusivity response to surface temperature change. This response is likely indirect, a result of snow cover, ground water, or vegetation cover differences that correspond with temperature change (Frob, 2011).

At 0.5m depth, there calculation thermal diffusivity maximum peaks in the spring, simultaneous with active layer thaw. This difference observed is likely the effect of latent heat on the calculation. The pattern of increase in calculated d_h due to latent heat of thawing at 0.5m is opposite to the decrease observed at 0.25m. Atmospheric temperature change seems to impact the measure d_h values at 0.5m. Generally, the global temperature

was rising from 2009 to 2015 (NOAA, 2017). 2009, the lowest global average temperature of all years in the data set, has only a very small peak in d_h during thaw, despite the fact the 0.5m is within the active layer. Additionally, the variability and d_h values increase in the winter each consecutive year, as global temperature also has increased.

At a borehole depth of 1.0m, the measured d_h values are around the minimum from mid summer to early fall. This corresponds the duration of time that the active layer is thawed. Thermal diffusivity peaks occur during freezing and thawing but, also when the active layer is completely frozen. Latent heat may be impacting the results during the time of freeze and thaw, but theoretically would not affect the calculations while the ground in completely frozen (Romanovsky and Osterkamp, 2000). It is therefore unclear what is influencing the timeing and extent of all calculated d_h changes throughout the time series.

At 1.5m, thermal diffusivity peaks occur right before the active layer thaws and decreases in d_h every year when the permafrost freezes. This is directly related to the latent heat. In 2010, the latter process is observed but, not the maximum during thaw. If the times of freeze and thaw are not considered, the measured thermal diffusivity seems to be increasing slightly with time. That is, the winter of 2013 to 2014 has higher d_h values than that of 2009 to 2010. This could be the result of a temperature related process, as average global temperature was rising over this time period.

Peaks in thermal diffusivity calculated at 2.5m depth mostly occur when the thaw depth reaches 2.5m in the summer due to latent heat release. The number of peaks, generally, increase as atmospheric temperature has increased. 2011, the Arctic warm anomaly year, was the first year to have three distinct d_h peaks. After that, each year has two or

three, while the prior years only had one. The additional peaks mostly occur right before permafrost thaw so, are still associated with latent heat. As all of these peaks are likely the result of latent heat release, this shows how the pattern of phase changes within the ground may change with increasing temperature.

Calculated thermal diffusivity at 3m depth has distinct minimums in the early spring, right before the ground thaws, and early fall, when the ground is freezing. Again, this draws direct correlation to latent heat effects. While the 3m depth is considered to remain frozen year round, it is likely that it is impacted by latent heat from depths directly above, which are within the active layer. Additionally, it is possible that, although the measured temperature is always below zero, liquid water may percolate to this depth and result is the presence of phase transitions. Some years have high d_h values in the winter while others have low values. It is not clear what causes this difference.

Even though the 5m borehole depth is well below the active layer, the calculated d_h values still have correspondence with timing of permafrost active layer thaw and, therefore, likely latent heat effects. The thermal diffusivity calculated decreases to minimum values at the point that the active layer is freezing. Most years, this is followed by a peak in d_h slightly higher than the values over the rest of the analysis time span. There is not correlation between yearly d_h patterns and external conditions as to determine the cause of more extreme minima or maxima.

10m depth has a year round temperature under $0^{\circ}\mathrm{C}$, experiences a yearly temperature variation of only $1^{\circ}\mathrm{C}$, and is 7m below the active layer. Still, the calculated d_h values correspond with the timing of the active layer condition and general temperature increase. 2009, the coldest year, little change in calculated d_h. Maximum d_h values, observed from

2010 onward, are always begin when the active layer thaws. This correlation implies the presence of latent heat release, but it is not clear how latent heat would cause a difference in calculated d_h as 10m depth is frozen year round. One possibility would be liquid water percolation through cracks in the bedrock, such as a joint. The length of time that the d_h value remains at the calculated maximum increases with each year, likely a result of the temperature change. The 10m also differs from the other depths, as the maximum calculated d_h is greater than any other depth analyzed by a factor of 10.

3.3.3 Conclusion

Throughout all results of thermal diffusivity for depths, there is correspondence between drastic d_h change and the permafrost thaw depth, indicating impact of latent heat on the ground heat transfer. This is surprising at 5m and 10m depth, which do not generally see phase transitions throughout the year. A possibility for this discrepancy is the percolation of liquid water from the active layer. This is consistent with the fact that in permafrost, liquid water and ice can exist in equilibrium at temperatures below O^{o}C (Osterkamp and Burn, 2003). The effect of latent heat is not consistent between depths. In some cases, it causes a peak in d_h and in others, a trough. Additionally, the amplitude of the latent heat related shifts is much different between depths. There are shifts in d_h by the same amplitude as those associated with latent heat release that do not correspond with timing of a thawed active layer. This brings question to what physical circumstances in which latent heat release will affect heat transfer, to what other processes may be affecting thermal diffusivity values, and how to distinguish the calculated d_h changes from true d_h changes

in the permafrost.

Several borehole depths exhibit d_h pattern differences over the six years of data, which may correlate with an increasing atmospheric temperature and permafrost average temperature. Temperature change may lead to a variety of condition changes such as snow cover, vegetation cover, and ground water amount or flow (Frob, 2011). Additionally, temperature change may trigger an increase in water percolation or amount of phase transitions that a depth experiences, inducing latent heat effects.

While the data analyzed is very informative to the effect of active layer freeze and thaw dynamics on the thermal properties throughout the borehole through latent heat, it is not telling to what and how other mechanisms may be altering thermal diffusivity. Latent heat definitely impacted the apparent thermal diffusivity. Based on the observed patterns that aligned with temperature rather than thawed depth, those that did not align with any known condition changes, and by the fact that the thermal diffusivity varies so greatly between depths, there are other components altering thermal diffusivity. Distinguishing the effects of latent heat on the d_h calculation from actual changes in thermal diffusivity, explaining the different mechanisms and effects of latent heat, and explaining the differences observed with depth is still needed. Clarity may be found if the experiment were repeated with better resolution in d_h test values, higher frequency of window start day, and if it were possible to use a smaller test window without losing root mean square error precision. Using this method to calculate thermal diffusivity the rest of the Kapp Linné 1 depths and at other boreholes would also increase understanding of the permafrost thermal properties. Specifically, analysis of a borehole that is in mineral based sediment rather than bedrock will allow for broader understanding of the permafrost

temperature profile. Creating an analysis that considered latent heat release would allow for evaluation of solely the thermal diffusivity changes.

Chapter 4

A More Complete Model

4.1 Motivation

A system of coupled ordinary differential equations is proposed to describe the permafrost system in detail through a mathematical model. The ground is treated as a series of finite ground layers and includes both the active layer and the permafrost. The atmosphere is treated as one cell directly in contact with the ground. The system of equations describe the changes of state that occur for a $1\mathrm{m}^2$ cross sectional area of the permafrost - atmosphere box model. Equations of state are given for ground temperature of n layers, ground carbon content of n layers, atmospheric temperature, atmospheric methane concentration, and atmospheric carbon dioxide concentration.

This is a general model with the purpose to evaluate the effect of the greenhouse gas radiative forcing and internal heat production system feedback mechanisms on the permafrost system and global climate. For sake of this analysis, simplifications and assumptions are made in the representation of the permafrost and climate system. Specifically,

groundwater flow is not considered. The model is additionally generalized in that it is not site specific. While the model is therefore not directly representative of a specific physical location, it offers greater information to understanding the system on a global scale.

4.2 Equations

4.2.1 Ground Temperature

The differential equation for ground temperature is given by Eq. 4.1. The subscript i denotes the ground layer, T is temperature in kelvin, and c_p is the specific heat capacity. The right hand side of Eq. 4.1 is composed of three components: conductivity, internal heat production, and latent heat.

$$c_p * \frac{dT_i}{dt} = \left[k\frac{T_{i+1} - 2T_i + T_{i-1}}{2\Delta z^2}\right] + AD(T_i, C_i) + Q_{latent} \tag{4.1}$$

Conductivity represents the heat transfer between layers due to difference in temperature. In the conductivity term, k is the thermal conductivity of the ground layer. Thermal conductivity is dependent on the material, unfrozen and frozen water content, temperature, and depth (Jansson and Karlberg, 2001).

Internal heat production is the heat increase of the ground due to organic decomposition processes (Hollesen et al., 2015). The main component of the internal heat production term is the function for decomposition $D(T_i, C_i)$. This is a Gaussian function, dependent on initial carbon content and temperature of the layer, that gives the mass of carbon decomposed in an individual layer. The coefficient, A, scales the decomposition function to give the amount of energy released from the organic carbon decomposition. A is esti-

mated as $3.9 * 10^7 \mathrm{Jg}^{-1}$ (Wieczorek et al., 2010).

The latent heat component, q_{latent} is the heat released during phase transitions within the permafrost. The impact on the heat transfer equation can be quite significant, shown in the thermal diffusivity analysis for Kapp Linné 1 to change the apparent thermal diffusivity by a up to a factor of 1000. The respective amounts of water and ice content are recognized to influence the amount of latent heat release. This may possibly be corresponded to differences in temperature and permafrost active layer thawing.

4.2.2 Ground Carbon Content

Eq. 4.2 is the differential equation for ground carbon content. The first term, $D(T_i, C_i)$, is the decomposition function, also presented Eq. 4.1. As it gives the amount of organic carbon decomposed, it represents mass of carbon leaving the ground layer as gas. The second term is the amount of organic carbon is deposited via litter fall, increasing ground carbon content.

$$\frac{dC_i}{dt} = -D_{CH_4}(T_i, C_i) - D_{CO_2}(T_i, C_i) + L(T_{atm}) \tag{4.2}$$

The decomposition function, $D(T_i, C_i)$, given in Eq. 4.3, gives the grams of carbon decomposed from an individual ground layer per day in terms of the initial amount of carbon present and the layer temperature. The Gaussian function, Eq. 4.4, is derived by experiment in Pietikainen et al. 2004., in which the decomposition rates for non-permafrost soils with analogous carbon content to permafrost were observed. The decomposition rates that result in production of methane and carbon dioxide have different Gaussian specifications in Eq. 4.4 so, are considered as two separate decomposition components in

the ground carbon equation of state (Treat et al., 2014).

$$D(T_i, C_i) = C_i r(T) \tag{4.3}$$

$$r(T) = \frac{a}{\sqrt{2\pi}} \exp\left(-\frac{b}{2}(T - T_c)^2 \right) \tag{4.4}$$

Litter fall is dependent on the atmospheric temperature as, vegetation activity increases with temperature and therefore sequesters more carbon into the ground (DeConto et al., 2012). This temperature dependence accounts for the seasonal variation is litter fall and also long term changes corresponding with global climate shifts. Litter fall for the i_{th} layer will vary, as surface vegetation deposits carbon into the upper ground layers only. Some carbon, however, may be shifted deeper into the permafrost through syngenetic permafrost growth and cryoturbation (Shur and Jorgenson, 2007).

4.2.3 Atmospheric Carbon Dioxide

Eq. 4.5 describes the change in local atmospheric carbon dioxide concentration through time.

$$\frac{d[\mathrm{CO_2}]}{dt} = f_{\mathrm{anth}}^{[\mathrm{CO_2}]}(t) + f_{\mathrm{seasonal}}^{[\mathrm{CO_2}]}(t) + \mathrm{ppm}_{\mathrm{CO_2}} \sum_{i=1}^{\mathrm{nlayers}} D_{\mathrm{CO_2}}(T_i, C_i) - b_{\mathrm{CO_2}}[\mathrm{CO_2}] - \mathrm{decay}_{\mathrm{CO_2}} \tag{4.5}$$

The first term, f_{anth}, is the amount of carbon dioxide that enters the atmosphere due to anthropogenic activity through time. The second term, $f_{seasonal}$, represents the global seasonal variation in atmospheric carbon dioxide content throughout one year. The third term is the carbon dioxide released into the atmosphere from decomposition of organic carbon in the ground. This is the summation of the amount of carbon dioxide released via organic decomposition in every ground layer, given by the decomposition $D(T, C)$. The

coefficient ppm_{CO_2} scales the decomposition function to give the change in atmospheric carbon dioxide in parts per million. The b_{CO_2} term represents the carbon dioxide that leaves the considered cell of atmosphere via diffusion. The last term, $decay_{CO_2}$, is an expression to describe how carbon dioxide molecules decay in the atmosphere (Muller and Muller, 2017). The expression for carbon dioxide remaining in the atmosphere after time t is $CO_2(t) = 0.217 + 0.259e^{\frac{-t}{172.9}} + 0.338e^{\frac{-t}{18.51}} + 0.186e^{\frac{-t}{1.186}}$ (Muller and Muller, 2017).

4.2.4 Atmospheric Methane

Eq. 4.6 describes the change in local atmospheric carbon concentration through time.

$$\frac{d[\mathrm{CH_4}]}{dt} = \mathrm{ppm_{CH_4}} \sum_{i=1}^{nlayers} D_{\mathrm{CH_4}}(T_i, C_i) - b_{\mathrm{CH_4}}[\mathrm{CH_4}] - \mathrm{decay_{CH_4}} \tag{4.6}$$

The first term is the methane released into the atmosphere from decomposition of organic carbon in the ground. This is the summation of the amount of methane released via organic decomposition in every ground layer, given by the decomposition $D(T, C)$. The coefficient ppm_{CH_4} scales the decomposition function to give the change in atmospheric methane in parts per million. The b_{CH_4} term represents the methane that leaves the considered cell of atmosphere via diffusion. The last term, $decay_{CH_4}$, is an expression to describe how methane molecules decay in the atmosphere (Muller and Muller, 2017). Atmospheric methane has a half life of 8.6 years (Muller and Muller, 2017).

4.2.5 Atmospheric Temperature

The equation for atmospheric temperature is given in Eq. 4.7. This is described with two terms, seasonal and greenhouse gas forcing.

$$\frac{dT_{atm}}{dt} = f^{T}_{seasonal}(t) + G(CO_2, CH_4) \tag{4.7}$$

The seasonal forcing term, $f_{seasonal}$, represents the annual variation in surface temperature due to the axial tilt of the Earth. The greenhouse gas forcing term, $G(CO_2, CH_4)$), gives the radiative effect of greenhouse gas heat absorption in the atmosphere (Hogg, 2008). Eq. 4.8 through Eq. 4.10 describe the components to the greenhouse gas forcing term. Eq. 4.8 gives the complete definition of $G(CO_2, CH_4)$. It is an additive function of a baseline atmospheric pre industrial greenhouse gas level, a function of the carbon dioxide concentration anomaly to pre industrial concentrations, and a function of the methane concentration anomaly. Eq. 4.9 and Eq. 4.10 describe the anomaly functions for carbon dioxide and methane, respectively (Hogg, 2008). Effective radiative forcing coefficients M_{CO_2} and M_{CH_4} scale the logarithmic anomalies to the corresponding change in energy that remains in the atmosphere. M_{CO_2} is estimated to be 20.5 Wm^{-2} (Hogg, 2008). M_{CH_4} is assesed to by 35 times greater than M_{CO_2} on a 20 year time scale (Ramaswamy et al., 1990).

$$c_a G = \bar{G} + G_{CO_2}(CO_2) + G_{CH_4}(CH_4) \tag{4.8}$$

$$G_{CO_2} = M_{CO_2} \ln\left(\frac{CO_2}{CO_{2o}}\right) \tag{4.9}$$

$$G_{CH_4} = M_{CH_4} \ln\left(\frac{CH_4}{CH_{4o}}\right) \tag{4.10}$$

Chapter 5

Conclusion

Recent anthropogenic influence on atmospheric greenhouse gas concentrations has led to an increase in global temperature (IPPC, 2014). Temperature increase is associated with warmer oceans, lower amount of snow and ice, sea level rise, and, among other impacts, thawing of the permafrost (IPPC, 2014). Permafrost is storage to about 1700 Gt of organic carbon which has potential to be released as carbon gas under thawing conditions (Knoblauch et al., 2018). Carbon dioxide and methane, both released from permafrost microbial decomposition, are potent greenhouse gases and would promote further increase in global temperature (Hansen et al., 2005). Permafrost thaw in geologic history has been linked to the extent of Quaternary interglacial periods and the PETM hyperthermals, confirming the large role permafrost plays in the carbon cycle and global climate (Zech, 2012). Yet, the permafrost influence has not been considered in either large scale predictions of the near future climate or in global anthropogenic greenhouse gas policy budgets. This thesis works towards better understanding of the permafrost system through evaluation of the temperature dependent microbial decomposition, thermal diffusivity analysis, and

proposal of a more complete permafrost model. The purpose of this is to work towards building a representative permafrost model that offers information about the near future permafrost conditions and their correlation with the global climate.

Permafrost decomposition rate function analysis was done through the Permafrost Bomb model, based off of the pre-existing Compost Bomb Instability model. The purpose of the Permafrost Bomb model is to increase understanding of, specifically, the long term decomposition rate ground temperature production feedback behavior. In the Permafrost Bomb model, the temperature dependent decomposition rate function was defined as a Gaussian function with maximum respiration rates at $40^{o}\mathrm{C}$. This was based on published lab analysis of soil respiration under varying incubation temperatures. The precise parameters that define the Gaussian are recognized to be an estimate, as lab analysis has not been done on specifically permafrost soils with incubation temperatures over $20^{o}\mathrm{C}$, meaning that the respiration at higher temperatures is not known with precision. The results from the Permafrost Bomb showed a series of system tipping points of decreasing amplitude over the 350 year modeling period and changed the temperature tipping peak shape. This resembles the post-PETM hyperthermal events, in which the global temperature had 6 rapid and significant peaks over the course of 3 million years (DeConto et al., 2012). The Permafrost Bomb results are significant as they are reflective of a more accurate decomposition rate function than previously proposed and support the hypothesis of permafrost involvement in the PETM hyperthermals.

The analysis of the Kapp Linne 1 borehole data for permafrost thermal diffusivity values was done to understand more about the inner permafrost heat exchange dynamics through time and depth. Results at all depths reflected the effect of latent heat on the

thermal diffusivity calculation, even at depths far below the active layer. Patterns were also observed at individual depths that did not align with timing of latent heat affect. Additionally, the variation in thermal diffusivity at different depths, and cyclically at one depth were very inconsistent. This raises question to the other processes within the permafrost and also to whether the effects from latent heat are completely understood. This experiment offered much information to the effect of latent heat on permafrost. To isolate changes in thermal diffusivity solely, a new method that considered latent heat would have to be created.

A more complete model for permafrost was proposed. This model included the interaction between a finite amount of permafrost depths as well as the atmosphere. The atmospheric consideration largely increases model complexity, as there are components of decay, diffusion, and that these dynamics differ for carbon dioxide and methane. The purpose of this model would be to model the permafrost system such that, information about the permafrost condition throughout the year can be determined and that the information obtained is applicable to the human lifespan. Much more research must be done on all terms mentioned in the proposed system of equations before attempting to build the model as a whole.

The current change in climate conditions has been compared to that during MIS 11 (Loutre and Berger, 2001). Understanding paleoclimate events, such as MIS 11 and the PETM, is vital to grasping how the global climate system, including permafrost, generally behave and are likely to behave in the future. Oppositely, observations that researchers make about the current state of the global climate system gives detail to processes recorded in the geologic history. Focus of permafrost research on both the long

term and short term scale is therefore necessary for system understanding. The three directions of research taken in this thesis add to the current understanding of the permafrost system and also lead to next possibilities in permafrost research, through focus on the long term interaction of decomposition rate and ground temperature, current thermal diffusivity patterns, and research compiled for an ideal permafrost model.

Bibliography

Christensen, T., Johansson, T., Akerman, H., Mastepanov, M., Malmer, N., Friborg, T., P, C. and Svensson, B. (2004), 'Thawing sub-arctic permafrost: Effects on vegetation and methane emissions', *Geophysical Research Letters* **31**, 1.

Christiansen, H. (2016), 'Kapp linne 1'.
URL: *http://gtnpdatabase.org/boreholes/view/57/*

Crichton, K., Roche, D., Krinner, G. and Chappellaz, J. (2014), 'A simplified permafrost-carbon model for long-term climate studies with the climber-2 coupled earth system model.', *Geoscientific Model Development* **7**, 3111.

DeConto, R. M., Galeotti, S., Pagani, M., Tracy, D., Schaefer, K., Zhang, T., Pollard, D. and Beerling, D. J. (2012), 'Past extreme warming events linked to massive carbon release from thawing permafrost', *Nature* **485**, 87.

Frob, K. (2011), Measuring and Modeling of Soil Thermal Properties and Ground Heat Flux at Two Different Sites at Lena Delta, Siberia., PhD thesis, University of Leiipzig Alfrd Wegener.

Hansen, J., Johnson, D., Lacis, A., Lebedeff, S., Lee, P., Rind, D. and Russell, G. (1981), 'Climate impact of increasing atmospheric carbon dioxide', *Science* **213**, 957.

Hansen, J., Sato, M., Reudy, R., Nazarenko, L., Lacis, A., Schmidt, G., Russell, G., Aleinov, I., Bauer, M., Bauer, S., Bell, N., Cairns, B., Canuto, V., Chandler, M., Cheng, Y., Genio, A. D., Faluvegi, G., Fleming, E., Friend, A., Hall, T., Jackman, C., Kelley, M., Kiang, N., Kock, D., Lean, J., Lerner, J., Lo, L., Menon, S., Miller, R., Minnis, P., Novakov, T., Oinas, V., Perlwitz, J., Perlwitz, J., Rind, D., Romanou, A., Schindell, D., Stone, P., Sun, S., Tausnev, N., Thresher, D., Wielicki, B., Wong, T., Yao, M. and Zhang, S. (2005), 'Efficacy of climate forcings.', *Journal of Geophysical Research* **110**, 1.

Hogg, A. M. (2008), 'Glacial cycles and carbon dioxide: A conceptual model', *Geophysical Research Letters* **35**, 1.

Hollesen, J., Matthiesen, H., Mollet, A. B. and Elberling, B. (2015), 'Permafrost thawing in organic arctic soils accelerated by ground heat production.', *Nature Climate Change* **5**, 574.

Hoyer-Leitzel, A., Nadeau, A., Roberts, A. and Steyer, A. (2017), 'Connections between

rate-induced tipping and nonautonomous stability theory'.

IPPC (2014), 'Climate change 2014 synthesis report summary for policymakers'.

Jansson, P. and Karlberg, L. (2001), 'Coupled heat and mass transfer model for soil-plant-atmosphere systems', *Royal Institute of Technology, Dept of Ciil and Environmental Engineering, Stokholm* p. 321.

Knoblauch, C., Beer, C., Liebner, S., Grigoriev, M. N. and Pfeiffer, E.-M. (2018), 'Methane production as key to the greenhouse gas budget of thawing permafrost.', *Nature Climate Change, Letters* .

Koven, C., Friedlingstein, P., Ciais, P., Khvorostyanov, D., Krinner, G. and Tarnocai, C. (2009), 'On the formation of high-latitude soil carbon stocks: Effects of cryoturbation and inslation by organic matter in a land surface model', *Geophysical Research Letters* **36**, 1.

Laurentano, V., Littler, K., Polling, M., Zachos, J. and Lourens, L. (2015), 'Frequency, magnitude and character of hyperthermal events at the onset of the early eocene climactic optimum.', *Climate of the Past* **11**, 1324.

Lee, S. (2012), 'Testing of the tropically excited arctic warming mechanism (team) with traditional el nino and la nina.', *American Meteorological Society* **4015**, 58.

Loutre, M. and Berger, A. (2001), 'Marine isotope stage 11 as an analogue for the present interglacial.', *GLobal and Planetary Change* **36**, 209.

Mikan, C. J., Schimel, J. . and Doyle, A. P. (2002), 'Temperature controld of microbial respiration in arcti tundra soils above and below freezing', *Soil Biology and Biochemistry* **34**, 1795.

Muller, R. A. and Muller, E. A. (2017), 'Fugitive methane and the role of atmospheric half life', *Geoinformatics and Geostatistics: An Overview* **5**.

NOAA (2017), 'Global climate report - annual 2017'.
URL: *https://www.ncdc.noaa.gov/sotc/global/201713*

NOAA (2018), 'Global climate change: Vital signs of the planet'.
URL: *https://climate.nasa.gov/vital-signs/carbon-dioxide/*

Osterkamp, T. and Burn, C. (2003), 'Permafrost', *Elsevier Science* p. 1728.

Pietikainen, J., Petterson, M. and Baath, E. (2004), 'Temperature controld of microbial respiration in arcti tundra soils above and below freezing', *FEMS Microbial Ecology* **52**, 58.

Ramaswamy, V., Leovy, C., Rodhe, H., Shine, K., Wange, W. and Wuebbles, D. (1990), 'Radiative forcing of climate', *NASA* .

Recktenwald, G. W. (2011), 'Finite difference approximations to the heat equation.', *Me-*

chanical Engineering **10**.

Romanovsky, V. and Osterkamp, T. (2000), 'Effects of unfrozen water on heat and mass transport processes in the active layer and permafrost.', *Permafrost. Permafrost and Periglacial Processes* **22**, 219.

Roth, K. and Boike, J. (2001), 'Quantifying the thermal dynamics of a permafrost site near ny-alesund, svalbard', *Water Resources Research* **37**, 2901.

Schaefer, K., Lantuir, H., Romanovsky, V. E., Schuur, E. A. and Witt, R. (2014), 'The impact of the permafrost carbon feedback on global climate', *Environmental Research Letters* **9**.

Schuur, E. A., Bockheim, J., Canadell, J. G., Euskirchen, E., Field, C. B., Goryachkin, S. V., Hagemann, S., Kuhry, O., Lafleur, O. M., Lee, H., Mazhitova, G., Nelson, F. E., Rinke, A., Romanovsky, V. E., nikolay Schiklomanov, Tarnocai, C., Venevsky, S., Vogel, J. G. and Zimov, S. A. (2008), 'Vulnerbility of permafrost carbon to climate change: Implications for the global carbon cycle', *Bioscience* **58**, 701.

Shur, Y. and Jorgenson, M. (2007), 'Patterns and permafrost formation and degradation in relation to climate and ecosystems', *Permafrost and Periglacial Processes* **18**, 19.

Treat, C., Wollheim, W., Varner, R., Grandy, A., Talbot, J. and Frolking, S. (2014), 'Temperature and peat type control co2 and ch4 production in alaskan permafrost peats', *Global Change Biology* **20**, 2674.

Vaks, A., Gutareva, O., Breitenbach, S., Avirmed, E., Mason, A., Osinzev, A. T. A., Kononov, A. and Henderson, G. (2013), 'Speleothems reveal 500,000 year history of siberian permafrost', *Science* **340**, 186.

Walz, J., Knoblauch, C., Bohme, L. and Pfeiffer, E.-M. (2017), 'Regulation of soil organic matter decompostition in permafrost affected siberian tundra soils - impact of oxygen availability, freezing and thawing, temperature, and labile organic matter', *Soil Biology and Biochemistry* **467**, 34.

Wieczorek, S., Ashwin, P., Luke, C. and Cox, P. (2010), 'Excitability in ramped systems: the compost-bomb instability', *Proceedings of the Royal Society* **467**, 1269.

Woo, M. (2012), *Permafrost Hydrology*, Springer-Verlag, Berlin Heidelberg.

Zech, R. (2012), 'A permafrost glacial hypothesis - permafrost carbon might help explaining the pleistocene ice ages', *Quaternary Science Journal* **61**, 92.